

Diffusion & Adversarial Schrödinger Bridges via Iterative Proportional Markovian Fitting

Sergei Kholkin^{*1} Grigoriy Ksenofontov^{*1,2} David Li^{*1} Nikita Kornilov^{*1,2} Nikita Gushchin^{*1}
Alexandra Suvorikova³ Alexey Kroshnin³ Evgeny Burnaev^{1,4} Alexander Korotin^{1,4}

Abstract

The Iterative Markovian Fitting (IMF) procedure, which iteratively projects onto the space of Markov processes and the reciprocal class, successfully solves the Schrödinger Bridge (SB) problem. However, an efficient practical implementation requires a heuristic modification—alternating between fitting forward and backward time diffusion at each iteration. This modification is crucial for stabilizing training and achieving reliable results in applications such as unpaired domain translation. Our work reveals a close connection between the modified version of IMF and the Iterative Proportional Fitting (IPF) procedure—a foundational method for the SB problem, also known as Sinkhorn’s algorithm. Specifically, we demonstrate that the heuristic modification of the IMF effectively integrates both IMF and IPF procedures. We refer to this combined approach as the Iterative Proportional Markovian Fitting (IPMF) procedure. Through theoretical and empirical analysis, we establish the convergence of IPMF procedure under various settings, contributing to developing a unified framework for solving SB problems.

1. Introduction

Diffusion models inspired by the Schrödinger Bridge (SB) theory, which connects stochastic processes with the optimal transport theory, have recently become powerful approaches in biology (Tong et al., 2024; Bunne et al., 2023), chemistry (Somnath et al., 2023; Igashov et al.), computer vision (Liu et al., 2023a; Shi et al., 2023) and speech processing (Chen et al., 2023). Most of these applications

^{*}Equal contribution ¹Skolkovo Institute of Science and Technology ²Moscow Institute of Physics and Technology ³Weierstrass Institute for Applied Analysis and Stochastics ⁴Artificial Intelligence Research Institute. Correspondence to: Sergei Kholkin <s.kholkin@skoltech.ru>, Nikita Gushchin <n.gushchin@skoltech.ru>, Alexander Korotin <a.korotin@skoltech.ru>.

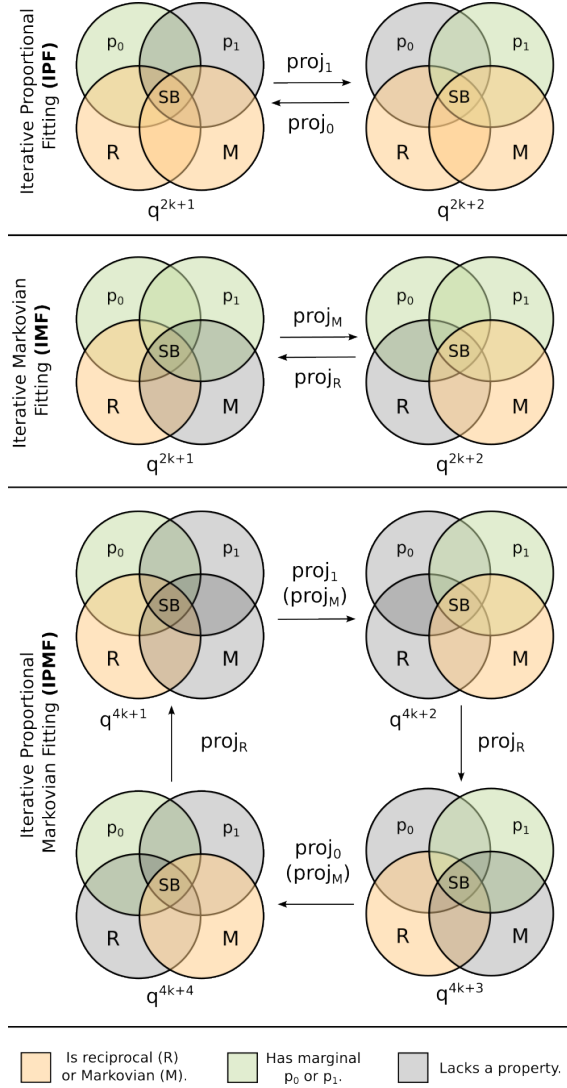


Figure 1: Diagrams of IPF, IMF, and unified IPMF procedure. All procedures aim to converge to the Schrödinger Bridge, i.e., the reciprocal and Markovian process with marginals p_0 and p_1 .

deal with either supervised domain translation, e.g., image super-resolution and inpainting (Liu et al., 2023a) or with unpaired translation, e.g., image style-transfer (Shi et al., 2023) or single-cell data analysis (Tong et al., 2024).

This work specifically focuses on *unpaired* domain translation (Zhu et al., 2017, Fig. 2). In this setting, given two domains represented solely by unpaired samples, the goal is to transform a sample from the input domain into a related sample from the target domain. In this context, researchers usually use SB-based algorithms because they enforce **two** key properties: *the optimality property*, ensuring similarity between the input and the translated object, and *the marginal matching property*, ensuring the translation of the input domain to the target domain.

Early works (De Bortoli et al., 2021; Vargas et al., 2021; Chen et al., 2021) on using the SB for unpaired domain translation employed the well-celebrated **Iterative Proportional Fitting** (IPF) procedure (Kullback, 1968), also known as the Sinkhorn algorithm (Cuturi & Doucet, 2014). The IPF procedure is initialized with a simple prior process satisfying the optimality property. It then refines this process iteratively through optimality-preserving transformations until the marginal matching property is achieved. In each iteration, IPF decreases the *forward* KL-divergence $\text{KL}(q^*||q)$ between the current approximation q and the ground-truth Schrödinger Bridge q^* . However, in practice, approximation errors may cause IPF to suffer from the “prior forgetting”, where the marginal matching property is achieved but optimality is lost (Vargas et al., 2024; 2021).

The **Iterative Markovian Fitting** (IMF) procedure (Shi et al., 2023; Peluchetti, 2023a; Gushchin et al., 2024) emerged as a promising competitor to IPF. Contrary to IPF, IMF starts from a stochastic process satisfying the marginal matching property and iteratively achieves optimality. Each iteration of IMF decreases the *reverse* KL-divergence $\text{KL}(q||q^*)$ between the current approximation q and the ground-truth Schrödinger Bridge q^* (cf. with IPF). The approach generalizes rectified flows (Liu et al., 2022) to stochastic processes, which are employed (Liu et al., 2023b; Yan et al., 2024) in modern foundational generative models such as Stable Diffusion 3 (Esser et al., 2024). Like IPF, IMF may also accumulate errors. Specifically, it may fail to approximate data distributions due to an imperfect fit at each iteration, causing the marginal matching property to be lost.

In practice, to stabilize IMF training and prevent error accumulation and loss of marginal matching property, practitioners use a heuristic modification of IMF. This is a bidirectional procedure alternating between learning forward and backward processes either by diffusion-based models in the **Diffusion** Schrödinger Bridge Matching (DSBM) algorithm (Shi et al., 2023) or GANs in **Adversarial** Schrödinger Bridge Matching (ASBM) algorithm (Gushchin et al., 2024).

In this work, we investigate the properties of the heuristic modification of IMF. **Our contributions are as follows:**

1. **Theory.** We show that the heuristic bidirectional IMF procedure used in practice is closely related to IPF—in fact, it *secretly* uses IPF iterations. Therefore, we propose calling the bidirectional IMF procedure **Iterative Proportional Markovian Fitting** (IPMF, §3.1). We prove that the IPMF procedure *exponentially* converges for Gaussians under various settings (§3.2). We *conjecture* that IPMF converges under very general settings offering a promising way of developing a unified framework for solving the SB problem.
2. **Practice.** We empirically validate our conjecture through a series of experiments, including the Gaussian setup (§4), toy 2D setups (§4.2), the Schrödinger Bridge benchmark (§4.3), setup with real-world colored MNIST and Celeba image data (§4.4).

These contributions demonstrate that the IPMF procedure has significant potential to **unify** a range of previously introduced SB methods—including IPF and IMF-based ones—in both discrete (Gushchin et al., 2024; De Bortoli et al., 2021) and continuous time (Shi et al., 2023; Peluchetti, 2023a; Vargas et al., 2021) settings, as well as their online versions (De Bortoli et al., 2024; Peluchetti, 2024; Karimi et al., 2024). Furthermore, the forward-backward IPMF framework could enable rectified flows to avoid error accumulation, making them even more powerful in generative modeling.

Notations. $\mathcal{P}_{2,ac}(\mathbb{R}^D)$ is a set of absolutely continuous distributions on \mathbb{R}^D with finite second moment and finite entropy. We fix $N \geq 1$ intermediate time moments and set $0 = t_0 < t_1 < \dots < t_N < t_{N+1} = 1$. Let $q \in \mathcal{P}_{2,ac}(\mathbb{R}^{D \times (N+2)})$ be an associated discrete stochastic process on this grid. For any such q , we denote the density at $(x_0, x_{t_1}, \dots, x_{t_N}, x_1) \in \mathbb{R}^{D \times (N+2)}$ as $q(x_0, x_{\text{in}}, x_1)$, with $x_{\text{in}} = (x_{t_1}, \dots, x_{t_N})$. W^ϵ is a Wiener process with volatility $\epsilon > 0$ and initial distribution p_0 . Let p^{W^ϵ} be its discretization, i.e.,
$$p^{W^\epsilon}(x_0, x_{\text{in}}, x_1) = p_0(x_0) \prod_{n=1}^{N+1} \mathcal{N}(x_{t_n} | x_{t_{n-1}}, \epsilon(t_n - t_{n-1})I_D),$$
 where $\mathcal{N}(\cdot|\cdot)$ is a conditional Gaussian distribution. KL is the Kullback-Leibler divergence; $H(q)$ is the differential entropy of q .

2. Background

This section details the study’s key concepts; §2.1 introduces the Schrödinger Bridge (SB) problem, §2.2 presents the Iterative Proportional Fitting (IPF), §2.3 describes the Iterative Markovian Fitting (IMF), §2.4 discusses the heuristic modification of the IMF (Bidirectional IMF).

Recall that the SB problem (Schrödinger, 1931), IPF and IMF admit both discrete– and continuous–time setups leading to the same problem solutions. Moreover, the explicit formulas for IPF and IMF in the discrete setup fa-

cilitate explaining our paper’s main idea. Thus, for the sake of presentation flow, **the main text focuses exclusively on the discrete setup**, while Appendix A presents the continuous setup.

2.1. Schrödinger Bridge (SB) Problem

The SB problem with a Wiener prior in the discrete-time setting (De Bortoli et al., 2021), given the initial distribution $p_0(x_0)$ and the final distribution $p_1(x_1)$, is stated as

$$\min_{q \in \Pi_N(p_0, p_1)} \text{KL}(q(x_0, x_{\text{in}}, x_1) \| p^{W^\epsilon}(x_0, x_{\text{in}}, x_1)), \quad (1)$$

where $\Pi_N(p_0, p_1) \subset \mathcal{P}_{2,ac}(\mathbb{R}^{D \times (N+2)})$ is the subset of discrete stochastic processes with marginals $q(x_0) = p_0(x_0)$, $q(x_1) = p_1(x_1)$. The objective function in (1) admits a decomposition

$$\begin{aligned} & \text{KL}(q(x_0, x_{\text{in}}, x_1) \| p^{W^\epsilon}(x_0, x_{\text{in}}, x_1)) = \\ & \text{KL}(q(x_0, x_1) \| p^{W^\epsilon}(x_0, x_1)) \\ & + \int \text{KL}(q(x_{\text{in}} | x_0, x_1) \| p^{W^\epsilon}(x_{\text{in}} | x_0, x_1)) q(x_0, x_1) dx_0 dx_1. \end{aligned}$$

All $q(x_{\text{in}} | x_0, x_1)$ can be chosen independently of $q(x_0, x_1)$. Thus, we can consider $q(x_{\text{in}} | x_0, x_1) = p^{W^\epsilon}(x_{\text{in}} | x_0, x_1)$ and get $\text{KL}(q(x_{\text{in}} | x_0, x_1) \| p^{W^\epsilon}(x_{\text{in}} | x_0, x_1)) = 0$. This leads to the **Static SB problem**:

$$\min_{q \in \Pi(p_0, p_1)} \text{KL}(q(x_0, x_1) \| p^{W^\epsilon}(x_0, x_1)), \quad (2)$$

where $\Pi(p_0, p_1) \subset \mathcal{P}_{2,ac}(\mathbb{R}^{D \times D})$ is the subset of joint distributions $q(x_0, x_1)$ s.t. $q(x_0) = p_0(x_0)$, $q(x_1) = p_1(x_1)$. Finally, we note that the static SB objective can be expanded as stated in (Gushchin et al., 2023a, Eq. 7),

$$\begin{aligned} & \text{KL}(q(x_0, x_1) \| p^{W^\epsilon}(x_0, x_1)) = \\ & \int \frac{\|x_1 - x_0\|^2}{2\epsilon} dq(x_0, x_1) - H(q(x_0, x_1)) + C, \quad (3) \end{aligned}$$

that is equivalent to the objective of the *entropic optimal transport* (EOT) problem with the *quadratic cost* up to an additive constant (Cuturi, 2013; Peyré et al., 2019; Léonard, 2013; Genevay, 2019).

2.2. Iterative Proportional Fitting (IPF)

Early works on SB (Vargas et al., 2021; De Bortoli et al., 2021) propose computational methods based on the IPF procedure (Kullback, 1968). The IPF-based algorithm is started by setting the process $q^0(x_0, x_{\text{in}}, x_1) = p_0(x_0)p^{W^\epsilon}(x_{\text{in}}, x_1|x_0)$. Then, the algorithm alternates between two types of IPF projections, proj_1 and proj_0 , given by (De Bortoli et al., 2021, Prop. 2):

$$q^{2k+1} = \text{proj}_1 \left(\underbrace{q^{2k}(x_1) \prod_{n=0}^N q^{2k}(x_{t_n} | x_{t_{n+1}})}_{q^{2k}(x_1)q^{2k}(x_0, x_{\text{in}} | x_1)} \right)$$

$$\stackrel{\text{def}}{=} p_1(x_1) \underbrace{\prod_{n=0}^N q^{2k}(x_{t_n} | x_{t_{n+1}})}_{q^{2k}(x_0, x_{\text{in}} | x_1)}, \quad (4)$$

$$\begin{aligned} q^{2k+2} &= \text{proj}_0 \left(\underbrace{q^{2k+1}(x_0) \prod_{n=1}^{N+1} q^{2k+1}(x_{t_n} | x_{t_{n-1}})}_{q^{2k+1}(x_0)q^{2k+1}(x_{\text{in}}, x_1 | x_0)} \right) \\ &\stackrel{\text{def}}{=} p_0(x_0) \underbrace{\prod_{n=1}^{N+1} q^{2k+1}(x_{t_n} | x_{t_{n-1}})}_{q^{2k+1}(x_{\text{in}}, x_1 | x_0)}. \quad (5) \end{aligned}$$

Thus, proj_1 and proj_0 replace marginal distributions $q(x_1)$ and $q(x_0)$ in $q(x_0, x_{\text{in}}, x_1)$ by $p_1(x_1)$ and $p_0(x_0)$ respectively. The constructed sequence $\{q^k\}$ converges to the solution of the SB problem q^* and causes the forward KL-divergence $\text{KL}(q^* \| q^k)$ to decrease monotonically at each iteration. In practice, since the prior process p^{W^ϵ} is used only for initialization, the imperfect fit may lead to a deviation from the SB solution at some iteration. This problem is called “prior forgetting” and was discussed in (Vargas et al., 2024, Appx. E.3). Vargas et al. (2021) consider a continuous analog of the IPF procedure using inversions of diffusion processes (see Appx. A.2).

2.3. Iterative Markovian Fitting (IMF)

The Iterative Markovian Fitting (IMF) procedure (Peluchetti, 2023a; Shi et al., 2023; Gushchin et al., 2024) emerged as a strong competitor to the IPF procedure. In contrast to IPF, IMF does not suffer from the “prior forgetting”. The procedure is initialized with any $q^0 \in \Pi_N(p_0, p_1)$. Then it alternates between reciprocal projection $\text{proj}_{\mathcal{R}}$ and Markovian projection $\text{proj}_{\mathcal{M}}$:

$$\begin{aligned} q^{2k+1} &= \text{proj}_{\mathcal{R}}(q^{2k}) \stackrel{\text{def}}{=} q^{2k}(x_0, x_1) p^{W^\epsilon}(x_{\text{in}} | x_0, x_1), \quad (6) \\ q^{2k+2} &= \text{proj}_{\mathcal{M}}(q^{2k+1}) \stackrel{\text{def}}{=} \underbrace{q^{2k+1}(x_0) \prod_{n=1}^{N+1} q^{2k+1}(x_{t_n} | x_{t_{n-1}})}_{\text{forward representation}} \\ &= \underbrace{q^{2k+1}(x_1) \prod_{n=0}^N q^{2k+1}(x_{t_n} | x_{t_{n+1}})}_{\text{backward representation}} \quad (7) \end{aligned}$$

The reciprocal projection $\text{proj}_{\mathcal{R}}$ creates a new (in general, non-Markovian) process combining the distribution $q(x_0, x_1)$ and $p^{W^\epsilon}(x_{\text{in}} | x_0, x_1)$. The latter is called the discrete Brownian Bridge. The Markovian projection $\text{proj}_{\mathcal{M}}$ uses the set of transitional densities $\{q(x_{t_n} | x_{t_{n-1}})\}$ or $\{q(x_{t_n} | x_{t_{n+1}})\}$ to create a new Markovian process starting from $q(x_0)$ or $q(x_1)$ respectively. The sequence $\{q^k\}$ converges to the solution of the SB problem q^* and causes the reverse KL-divergence $\text{KL}(q^k \| q^*)$ to decrease monotonically at each iteration (cf. with IPF). Shi et al. (2023);

Peluchetti (2023a) consider a continuous-time version of the IMF (see Appx. A.3).

2.4. Heuristic bidirectional modification of IMF

The result of the Markovian projection (7) admits both forward and backward representation. To learn the corresponding transitional densities, one uses neural networks $\{q_\theta(x_{t_n}|x_{t_{n-1}})\}$ (**forward parametrization**) or $\{q_\phi(x_{t_n}|x_{t_{n+1}})\}$ (**backward parametrization**). The starting distributions are as follows: $q_\theta(x_0) = p_0(x_0)$ for the forward parametrization and $q_\phi(x_1) = p_1(x_1)$ for the backward parametrization. In practice, the alternation between forward and backward representations of Markovian processes is used in both implementations of continuous-time IMF by **DSBM** algorithm (Shi et al., 2023, Alg. 1) based on diffusion models and discrete-time IMF by **ASBM** algorithm (Gushchin et al., 2024, Alg. 1) based on the GANs. This **bidirectional** procedure can be described as follows:

$$\begin{aligned}
 q^{4k+1} &= \underbrace{q^{4k}(x_0, x_1)p^{W^\epsilon}(x_{\text{in}}|x_0, x_1)}_{\text{proj}_{\mathcal{R}}(q^{4k})}, \\
 q^{4k+2} &= p(x_1) \underbrace{\prod_{n=0}^N q_\phi^{4k+1}(x_{t_n}|x_{t_{n+1}})}_{\text{backward parametrization}}, \quad (8) \\
 q^{4k+3} &= \underbrace{q^{4k+2}(x_0, x_1)p^{W^\epsilon}(x_{\text{in}}|x_0, x_1)}_{\text{proj}_{\mathcal{R}}(q^{4k+1})}, \\
 q^{4k+4} &= p(x_0) \underbrace{\prod_{n=1}^{N+1} q_\theta^{4k+3}(x_{t_n}|x_{t_{n-1}})}_{\text{forward parametrization}}. \quad (9)
 \end{aligned}$$

Thus, only one marginal is fitted perfectly, e.g., $q_\theta(x_0) = p_0(x_0)$ in the case of forward representation, while the other marginal is only learned, e.g., $q_\theta(x_1) = \int \underbrace{q_\theta(x_0)}_{=p_0(x_0)} \prod_{n=1}^{N+1} q_\theta(x_{t_n}|x_{t_{n-1}}) dx_0 dx_1 \cdots dx_N \approx p_1(x_1)$.

Shi et al. (2023); Peluchetti (2023a); Gushchin et al. (2024) observed that the bidirectional IMF does not accumulate approximation errors (see §2.3), while the use of only forward or only backward parametrization accumulates errors and leads to divergence (De Bortoli et al., 2024, Appx. I).

3. Iterative Proportional Markovian Fitting

This section demonstrates that the heuristic bidirectional IMF (§2.4) is, in fact, the alternating implementation of IPF and IMF projections. §3.1 establishes that this heuristic defines the unified Iterative Proportional Markovian Fitting (IPMF) procedure. §3.2 provides the analysis of the convergence of the IPMF procedure under various settings.

3.1. Bidirectional IMF is IPMF

Here, we analyze the structure of the heuristic bidirectional IMF. For a given Markovian process q , we recall that its IPF

projections ($\text{proj}_0(q)$ (5) and $\text{proj}_1(q)$ (4)) replace the starting distribution $q(x_0)$ with $p_0(x_0)$ and $q(x_1)$ with $p_1(x_1)$, respectively. Further, the process q^{4k+2} (8) is a result of a combination of the Markovian projection $\text{proj}_{\mathcal{M}}$ (7) in forward parametrization and of the IPF projection proj_1 (4):

$$\begin{aligned}
 q^{4k+2} &= p(x_1) \prod_{n=0}^N q^{4k+1}(x_{t_n}|x_{t_{n+1}}) \\
 &= \underbrace{\text{proj}_1 \left(q^{4k+1}(x_1) \prod_{n=0}^N q^{4k+1}(x_{t_n}|x_{t_{n+1}}) \right)}_{\text{proj}_1(\text{proj}_{\mathcal{M}}(q^{4k+1}))}.
 \end{aligned}$$

Next, the process q^{4k+4} (9) results from a combination of the Markovian projection $\text{proj}_{\mathcal{M}}$ (7) in backward parametrization and of the IPF projection proj_0 (5):

$$\begin{aligned}
 q^{4k+3} &= p(x_0) \prod_{n=1}^{N+1} q^{4k+3}(x_{t_n}|x_{t_{n-1}}) \\
 &= \underbrace{\text{proj}_0 \left(q^{4k+3}(x_0) \prod_{n=1}^{N+1} q^{4k+3}(x_{t_n}|x_{t_{n-1}}) \right)}_{\text{proj}_0(\text{proj}_{\mathcal{M}}(q^{4k+3}))}.
 \end{aligned}$$

Thus, we can represent the heuristic bidirectional IMF given by (9) and (8) as follows:

Iterative Proportional Markovian Fitting (Discrete time)

$$\begin{aligned}
 q^{4k+1} &= \underbrace{q^{4k}(x_0, x_1)p^{W^\epsilon}(x_{\text{in}}|x_0, x_1)}_{\text{proj}_{\mathcal{R}}(q^{4k})}, \\
 q^{4k+2} &= p(x_1) \underbrace{\prod_{n=0}^N q^{4k+1}(x_{t_n}|x_{t_{n+1}})}_{\text{proj}_1(\text{proj}_{\mathcal{M}}(q^{4k+1}))}, \\
 q^{4k+3} &= \underbrace{q^{4k+2}(x_0, x_1)p^{W^\epsilon}(x_{\text{in}}|x_0, x_1)}_{\text{proj}_{\mathcal{R}}(q^{4k+1})}, \\
 q^{4k+4} &= p(x_0) \underbrace{\prod_{n=1}^{N+1} q^{4k+3}(x_{t_n}|x_{t_{n-1}})}_{\text{proj}_0(\text{proj}_{\mathcal{M}}(q^{4k+3}))}.
 \end{aligned}$$

The heuristic bidirectional IMF alternates between two IMF projections ($\text{proj}_{\mathcal{M}}(\text{proj}_{\mathcal{R}}(\cdot))$) during which the process “became more optimal” (step towards optimality property) and two IPF projections (proj_0 and proj_1) during which the marginal fitting improves (step towards marginal matching property). For this reason, we refer to the bidirectional IMF, which can start from any initial process $q^0(x_0, x_{\text{in}}, x_1)$, as **Iterative Proportional Markovian Fitting (IPMF)**. An *IPMF step* consists of two IMF projections and two IPF projections. We hypothesize that IPMF converges from any initial process $q^0(x_0, x_{\text{in}}, x_1)$, unlike IPF and IMF, which require a specific form of the starting

process. We emphasize that IPMF reduces to IMF when the initial coupling is reciprocal and has the correct marginals p_0 and p_1 . Similarly, if the initial coupling is Markovian, reciprocal and has the correct initial marginal p_0 or p_1 , then IPMF reduces to IPF. Fig. 1 visualizes these cases, clarifying the role of the initial coupling and the iterative steps. A similar analysis for continuous-time IPMF is provided in Appx. A.3.

3.2. Theoretical Convergence Analysis for Gaussians

Our first result introduces a novel approach to quantify the optimality property for a Gaussian plan. We show that any $2D$ Gaussian distribution ($D \geq 1$) is an entropic OT plan between its marginals for a certain transport cost. Let $\Sigma, \tilde{\Sigma} \in \mathbb{R}^{D \times D}$ be positive definite matrices ($\Sigma, \tilde{\Sigma} \succ 0$) and $P \in \mathbb{R}^{D \times D}$ be s.t. $\Sigma - P(\tilde{\Sigma})^{-1}P^\top \succ 0$. Define

$$\Xi(P, \Sigma, \tilde{\Sigma}) \stackrel{\text{def}}{=} (\tilde{\Sigma})^{-1}P^\top (\Sigma - P(\tilde{\Sigma})^{-1}P^\top)^{-1}. \quad (10)$$

Theorem 3.1. *Let $q(x_0, x_1)$ be Gaussian with marginals $p = \mathcal{N}(\mu, \Sigma)$ and $\tilde{p} = \mathcal{N}(\tilde{\mu}, \tilde{\Sigma})$,*

$$q(x_0, x_1) = \mathcal{N}\left(\begin{pmatrix} \mu \\ \tilde{\mu} \end{pmatrix}, \begin{pmatrix} \Sigma & P \\ P^\top & \tilde{\Sigma} \end{pmatrix}\right).$$

Let $A = \Xi(P, \Sigma, \tilde{\Sigma})$. Then q is the unique minimizer of

$$\min_{q' \in \Pi(p, \tilde{p})} \left\{ \int (-x_1^\top A x_0) \cdot q'(x_0, x_1) dx_0 dx_1 - H(q') \right\}. \quad (11)$$

Problem (11) is the OT problem with the transport cost $c_A(x_0, x_1) := -x_1^\top A x_0$ and entropy regularization (with weight 1) (Cuturi, 2013; Genevay, 2019). In other words, for any $2D$ Gaussian distribution q , there exists a matrix $A(q) \in \mathbb{R}^{D \times D}$ that defines the cost function for which q solves the EOT problem. We name $A(q)$ the **optimality matrix**. If q is s.t. $A(q) = \epsilon^{-1}I_D$, then the corresponding transport cost is $c_A(x_0, x_1) = -\epsilon^{-1} \cdot \langle x_1, x_0 \rangle$ which is equivalent to $\epsilon^{-1} \cdot \|x_1 - x_0\|^2/2$. Consequently, q is the static SB (2) between its marginals $q_0(x_0)$ and $q_1(x_1)$ for the prior W^ϵ , recall (3).

Main result. We prove the exponential convergence of IPMF (w.r.t. the parameters) to the solution q^* of the static SB problem (2) between p_0 and p_1 under certain settings. .

Theorem 3.2 (Convergence of IPMF for Gaussians). *Let $p_0 = \mathcal{N}(\mu_0, \Sigma_0)$ and $p_1 = \mathcal{N}(\mu_1, \Sigma_1)$ be D -dimensional Gaussians. Assume that we run IPMF with volatility $\epsilon > 0$, starting from some 2D Gaussian¹*

$$q^0(x_0, x_1) = \mathcal{N}\left(\begin{pmatrix} \mu_0 \\ \nu \end{pmatrix}, \begin{pmatrix} \Sigma_0 & P_0 \\ P_0 & S_0 \end{pmatrix}\right) \in \mathcal{P}_{2,ac}(\mathbb{R}^D \times \mathbb{R}^D).$$

We denote the distribution obtained after k IPMF steps by

¹We assume that $q^0(x_0) = p_0(x_0)$, i.e., the initial process starts at p_0 at time $t = 0$. This is reasonable, as after the first IPMF round the process will satisfy this property thanks to the IPF projections involved.

$$q^{4k}(x_0, x_1) \stackrel{\text{def}}{=} \mathcal{N}\left(\begin{pmatrix} \mu_0 \\ \nu_k \end{pmatrix}, \begin{pmatrix} \Sigma_0 & P_k \\ P_k & S_k \end{pmatrix}\right) \in \mathcal{P}_{2,ac}(\mathbb{R}^D \times \mathbb{R}^D)$$

and $A_k \stackrel{\text{def}}{=} \Xi(P_k, \Sigma_0, S_k)$. Then in the following settings

- $D = 1$, IMF or D -IMF ($N = 1$), any $\epsilon > 0$;
- $D > 1$, D -IMF ($N = 1$), $\epsilon \gg 0$ (see Appendix B.5);

the following exponential convergence bounds hold:

$$\begin{aligned} \|S_k^{-\frac{1}{2}}\Sigma_1 S_k^{-\frac{1}{2}} - I_D\|_2 &\leq \alpha^{2k} \|S_0^{-\frac{1}{2}}\Sigma_1 S_0^{-\frac{1}{2}} - I_D\|_2, \\ \|\Sigma_1^{-\frac{1}{2}}(\nu_k - \mu_1)\|_2 &\leq \alpha^k \|\Sigma_1^{-\frac{1}{2}}(\nu_0 - \mu_1)\|_2, \\ \|A_k - \epsilon^{-1}I_D\|_2 &\leq \beta^{2k} \|A_0 - \epsilon^{-1}I_D\|_2, \end{aligned} \quad (12)$$

with $\alpha, \beta < 1$ and $\|\cdot\|_2$ being the spectral norm; α, β depend on IPMF type (discrete or continuous), initial parameters S_0, ν_0, P_0 , marginal distributions p_0, p_1 and ϵ . Consequently, $KL(q^{4k} \| q^*)$, $KL(q^* \| q^{4k}) \xrightarrow{k \rightarrow \infty} 0$.

Proof details. We find that IPF step preserves the optimality matrix A_k (L. B.3) and improves the marginal matching property for $q(x_0, x_1)$ (L. B.1). Next, we analyze closed formulas for IMF step in the Gaussian case (Peluchetti, 2023a; Gushchin et al., 2024) and show that the IMF step makes A_k closer to $\epsilon^{-1}I_D$ (preserving marginals of q^{4k}). Namely, we verify the contractivity of each step w.r.t. A_k .

General conjecture. *We believe that IPMF converges under very general settings (far beyond the Gaussian case). Moreover, in the Gaussian case, we expect exponential convergence for all $\epsilon > 0$, all D , and all IMF types. We verify these claims experimentally (§4).*

4. Experimental Illustrations

This section provides empirical evidence that IPMF converges under a more general setting—specifically, from any starting process—unlike IPF and IMF. The goal is to achieve the same or similar results across all used starting coupling and for both discrete-time (ASBM) and continuous-time (DSBM) solvers. §3.1 and Appx. A show that the bidirectional IMF and the proposed IPMF differ only in the initial starting process. Since both practical implementations of continuous-time IMF (Shi et al., 2023, Alg. 1) and discrete-time IMF (Gushchin et al., 2024, Alg. 1) use the considered bidirectional version, we use practical algorithms introduced in these works, i.e., Diffusion Schrödinger Bridge Matching (**DSBM**) and Adversarial Schrödinger Bridge Matching (**ASBM**) respectively.

Experimental setups. We consider multivariate Gaussian distributions for which we have closed-form IPMF update formulas §4, an illustrative 2D example, the Schrödinger Bridges Benchmark (Gushchin et al., 2023b) and real-life image data distributions, i.e., the colored

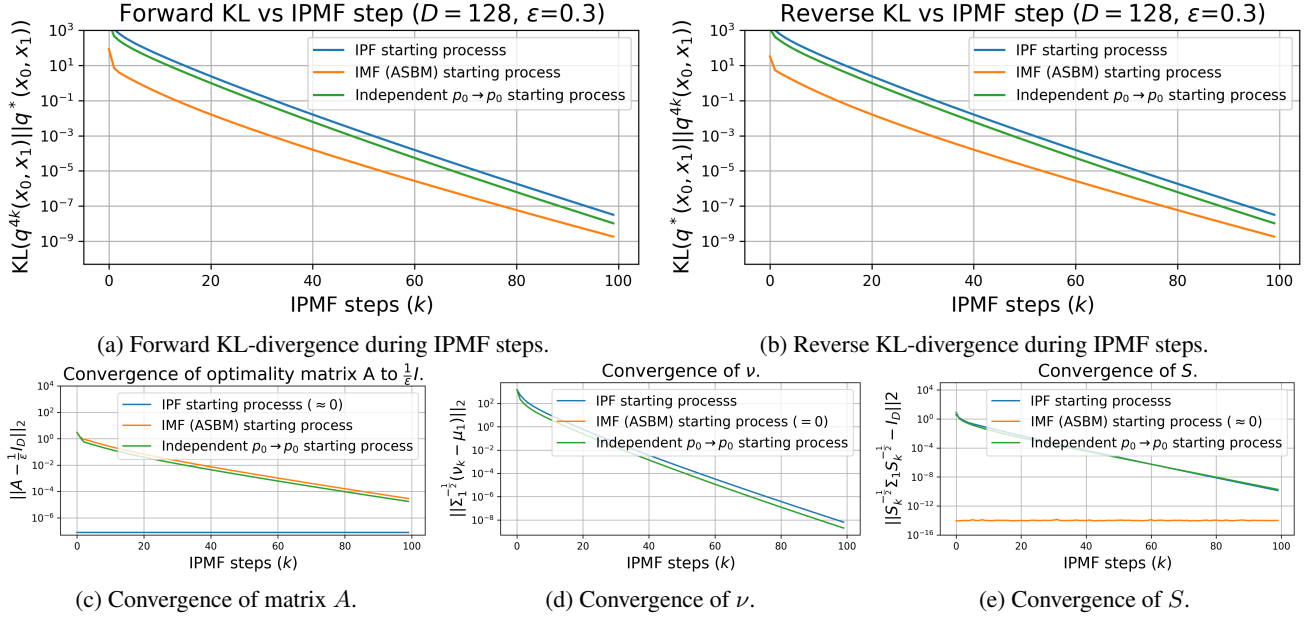


Figure 2: Convergence of IPMF procedure with different starting process q^0 .

MNIST dataset and the Celeba dataset (Liu et al., 2015). All technical details can be found in the Appx. C.

Starting processes. We focus on running the IPMF procedure from various initializations, referred to as *starting processes*. The starting processes are constructed by selecting different couplings $q^0(x_0, x_1)$ and incorporating the Brownian Bridge process $W_{|x_0, x_1}^\epsilon$ (i.e., W^ϵ conditioned on x_0, x_1). In the discrete-time setup, for each selected coupling $q^0(x_0, x_1)$ we construct the starting process as $q^0(x_0, x_{in}, x_1) = q^0(x_0, x_1)p^{W^\epsilon}(x_{in}|x_0, x_1)$ and $T^0 = \int W_{|x_0, x_1}^\epsilon dq^0(x_0, x_1)$ for the continuous-time case (see Appx. A). We consider three “starting” scenarios: IMF-like starting process of the form $q^0(x_0, x_1) = p_0(x_0)p_1(x_1)$, IPF-like starting process of the form $q^0(x_0, x_1) = p_0(x_0)p^{W^\epsilon}(x_1|x_0)$, and various starting processes which cannot be used to initialize IMF or IPF. The latter demonstrates that IPMF converges under a more general setting.

The results of DSBM and ASBM algorithms starting from different starting processes are denoted as (D/A)SBM-*name of coupling*, e.g., the results for the DSBM using the IMF starting process would be denoted as DSBM-IMF.

4.1. High Dimensional Gaussians

This section experimentally validates the convergence of IPMF for the multivariate Gaussians (see our **General conjecture**). We use explicit formulas for the discrete IMF (Gushchin et al., 2024, Thm. 3.8) and follow the setup from (Gushchin et al., 2023a, Sec. 5.2). Specifically, we consider SB problem with $D = 128$ and $\epsilon = 0.3$ for centered Gaussians, $p_0 = \mathcal{N}(0, \Sigma_0)$ and $p_1 = \mathcal{N}(0, \Sigma_1)$. The eigenvectors of Σ_0 and Σ_1 are sampled from the uniform

distribution on the unit sphere. Their eigenvalues are sampled from the loguniform distribution on $[-\log 2, \log 2]$. We choose $N = 3$ intermediate time points uniformly between $t = 0$ and $t = 1$ and run 100 steps of the IPMF procedure, each consisting of two IPF projections and two Markovian-Reciprocal projections (see §3.1). Denote as $q^{4k} = q^{4k}(x_0, x_1)$ the IPMF output at the k -th step and let $q^* = q^*(x_0, x_1)$ be the solution of the static SB. Fig. 2 shows that both the forward KL ($q^* || q^{4k}$) and reverse KL ($q^{4k} || q^*$) divergences converge. The quantities from (12) converge to zero exponentially, as expected.

4.2. Illustrative 2D example

We consider the SB problem with $\epsilon = 0.1$, p_0 being Gaussian distribution on \mathbb{R}^2 and p_1 being the Swiss roll. We train DSBM and ASBM algorithms using IMF and IPF starting processes. Additionally, we consider *Ind* $p_0 \rightarrow p_0$ starting processes induced by $q^0(x_0, x_1) = p_0(x_0)p_0(x_1)$. Fig. 7 presents the starting processes and the results. In all the cases, we observe convergence to the target distribution.

4.3. Evaluation on the SB Benchmark

We use the SB mixtures benchmark (Gushchin et al., 2023b) with the ground truth solution to the SB problem to test ASBM and DSBM with IMF, IPF, and *Ind* $p_0 \rightarrow p_0$ as the starting processes. The benchmark provides continuous distribution pairs p_0, p_1 for dimensions $D \in \{2, 16, 64, 128\}$ that have known SB solutions for volatility $\epsilon \in \{0.1, 1, 10\}$. To evaluate the quality of the recovered SB solutions, we use the cBWW₂-UVP metric (Gushchin et al., 2023b). Tab. 1 provides the results. Appx. C shows how all the approaches learn the target distribution.

		$\epsilon = 0.1$				$\epsilon = 1$				$\epsilon = 10$				
Algorithm Type		$D=2$	$D=16$	$D=64$	$D=128$	$D=2$	$D=16$	$D=64$	$D=128$	$D=2$	$D=16$	$D=64$	$D=128$	
Best algorithm on benchmark [†]		Varies	1.94	13.67	11.74	11.4	1.04	9.08	18.05	15.23	1.40	1.27	2.36	1.31
	DSBM-IMF		1.21	4.61	9.81	19.8	0.68	0.63	5.8	29.5	0.23	5.45	68.9	362
	DSBM-IPF		2.55	17.4	15.85	17.45	0.29	0.76	4.05	29.59	0.35	3.98	83.2	210
	DSBM- $Ind(p_0, p_0)$		2.72	11.7	16.5	17.02	0.41	0.92	3.7	29	0.16	3.91	101	255
	ASBM-IMF [†]	IPMF	0.89	8.2	13.5	53.7	0.19	1.6	5.8	10.5	0.13	0.4	1.9	4.7
	ASBM-IPF		3.06	14.37	44.35	32.5	0.18	1.68	9.25	20.47	0.13	0.36	2.28	4.97
	ASBM- $Ind(p_0, p_0)$		3.99	15.73	39.3	40.32	0.18	1.68	6.16	12.8	0.13	0.38	1.36	2.6
	SF ² M-Sink [†]		0.54	3.7	9.5	10.9	0.2	1.1	9	23	0.31	4.9	319	819

Table 1: Comparisons of cBW_2^2 -UVP \downarrow (%) between the static SB solution $q^*(x_0, x_1)$ and the learned solution on the SB benchmark. The best metric is **bolded**. Results marked with [†] are taken from (Gushchin et al., 2024) and (Gushchin et al., 2023b). The results of DSBM and ASBM algorithms starting from different starting processes are denoted as (D/A)SBM-**name of starting process**.

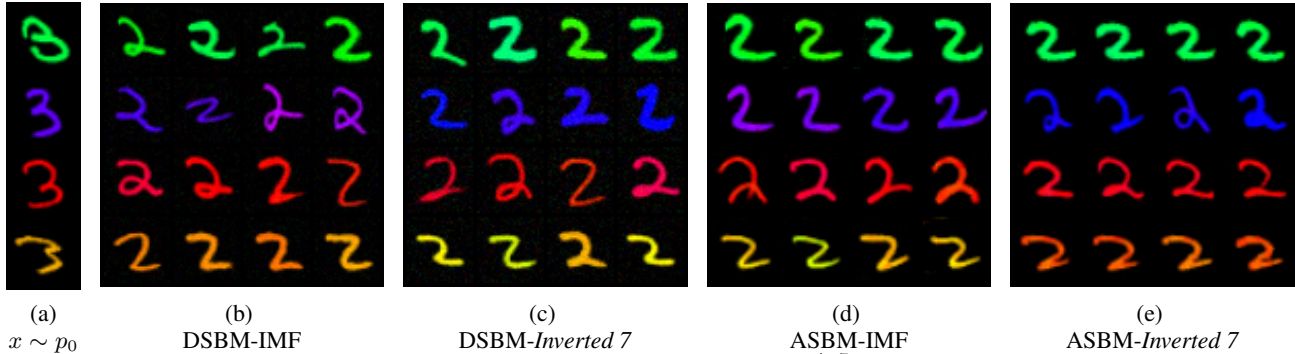


Figure 3: Samples from DSBM and ASBM learned with IPMF using IMF and q^{inv7} starting processes on Colored MNIST 3 \rightarrow 2 (32×32) translation for $\epsilon = 10$.

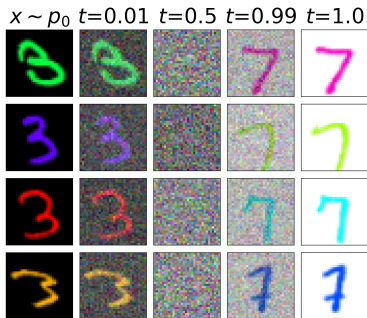


Figure 4: *Inverted 7* starting process, i.e., reciprocal process with marginals p_0 and p^{inv7} , visualization.

DSBM and ASBM starting from all the processes at $\epsilon \in \{1, 10\}$ yield quite similar results. If $\epsilon = 0.1$, DSBM and ASBM with IPF and $Ind p_0 \rightarrow p_0$ starting processes the quality decreases slightly.

4.4. Unpaired Image-to-Image translation

To test IPMF on real data, we consider two unpaired image-to-image translation setups: *colored 3* \rightarrow *colored 2* digits from the MNIST dataset with 32×32 resolution size and *male* \rightarrow *female* faces from the Celeba dataset with 64×64 resolution size.

Colored MNIST. We construct train and test sets by RGB colorization of MNIST digits from corresponding train and test sets of classes "2" and "3". We train ASBM and DSBM algorithms starting from the IMF process. Addi-

tionally, we test a starting process induced by the independent coupling of the distribution of colored digits of class "3" (p_0) and the distribution of colored digits of class "7" with inverted RGB channels ($p^{inv7}(x_1)$). We refer to this process as *Inverted 7*, i.e., $q^0(x_0, x_1) = p_0(x_0)p^{inv7}(x_1)$ (see Fig. 4). Appx. C contains further technical details. We learn DSBM and ASBM on the *train* set of digits and visualize the translated *test* images (Fig. 3).

Both DSBM and ASBM algorithms starting from both IMF and *Inverted 7* starting process fit the target distribution of colored MNIST digits of class "2" and preserve the color of the input image during translation. This supports that the limiting behavior of IPMF resembles the solution of SB.

Celeba. We consider the IMF-OT variation of the IMF starting process. It is induced by a mini-batch optimal transport coupling $q^{OT}(x_0, x_1)$ (Tong et al., 2024). We also test $Ind p_0 \rightarrow p_0$ starting process. Additionally, we test starting processes induced by *DDPM SDEdit* and *SD SDEdit* couplings, which is the SDEdit method (Meng et al., 2021) used for *male* \rightarrow *female* translation with (1) DDPM (Ho et al., 2020) model trained on the female part of Celeba and (2) *Stable Diffusion* v1.5 (Rombach et al., 2022) with designed text prompt, see Appx. C.3. We use approximately the same number of parameters for DSBM and ASBM generator and 10% of male and female images as a test set for evaluation (see Appx. C other details). Fig. 5 provides qualitative results. To analyze them quantitatively, we plot FID as a function of number of IPMF

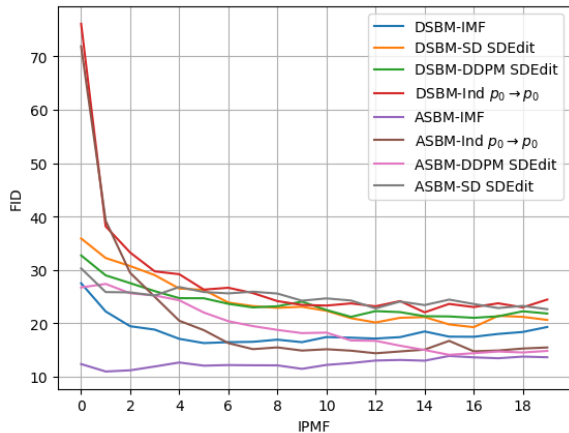
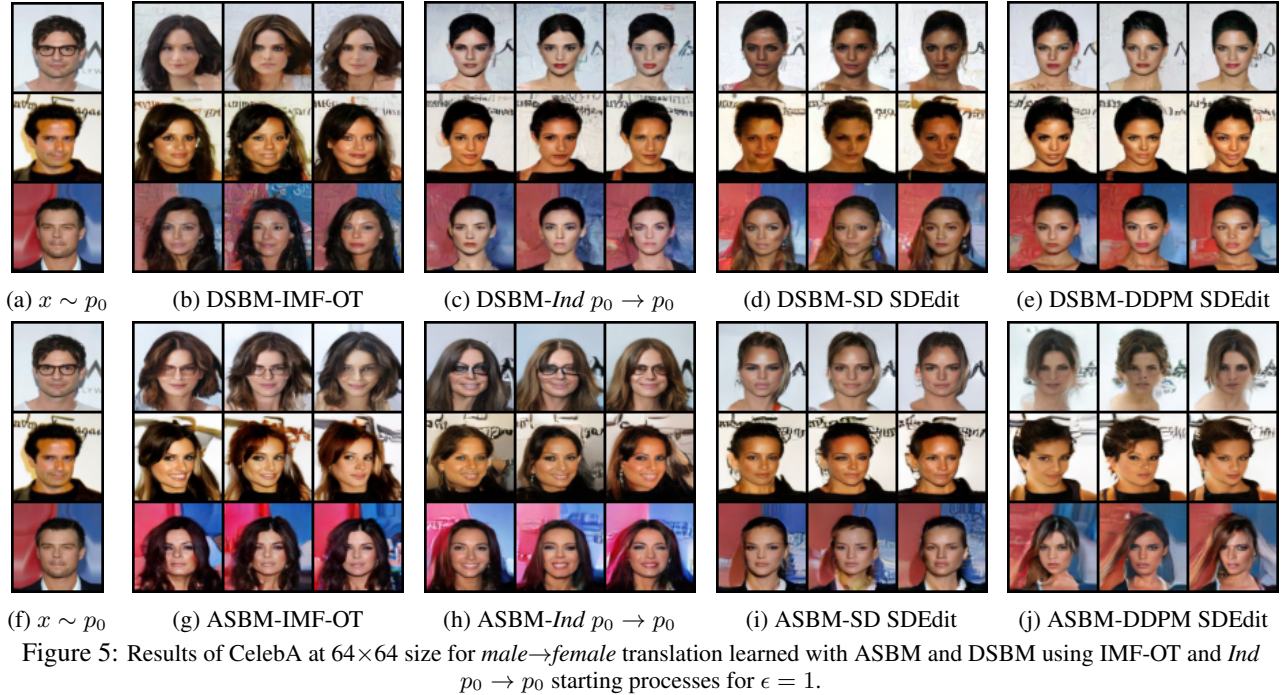


Figure 6: Convergence of models to target distribution. FID plotted as a function of IPMF iterations for all the presented setups.

iterations (Fig. 6). Fig. 5 shows that the presented models: (1) converge to the target distribution, (2) keep alignment between the features of the input images and generated images (e.g., hair color, background, etc.). However, the samples generated by these models differ, since different initial conditions produce distinct neural network optimization trajectories. Thus, some starting processes give a better fit to the target distribution (FID plot, Fig. 6), and some of them preserve better the input image features (MSE plot, Fig. 8b). FID plot (Fig. 6) shows that all the models fit the target distribution quite well. MSE plot (Fig. 8b) together with generated samples (Fig. 5) demonstrate that the *SDEdit* starting processes yield high similarity between images before and after translation, than the other starting

processes. At the same time, the quality of fitting the target distribution remains comparable for all the cases.

5. Discussion

Potential impact. The IPMF procedure demonstrates a potential to overcome the error accumulation problem observed in distillation methods—such as rectified flows (Liu et al., 2022; 2023b)—which are used to accelerate foundational image generation models like StableDiffusion 3 in (Esser et al., 2024). These distillation methods are the limit of one-directional IMF procedure with $\epsilon \rightarrow 0$. The one-directional version accumulates errors, which may lead to the divergence (De Bortoli et al., 2024, Appx. I). The use of the bidirectional version (with $\epsilon > 0$) should correct the marginals and make diffusion trajectories more straight to accelerate the inference of diffusion models. We believe that considering such distillation techniques from the IPMF point of view may help to overcome the current limitations of these techniques.

Limitations. While we show the proof of exponential convergence of the IPMF procedure in the Gaussian case in various setting, and present a wide set of experiments supporting this procedure, the proof its convergence in the general case still remains a promising avenue for future work.

6. Broader impact.

This paper presents work whose goal is to advance the field of Machine Learning. There are many potential societal consequences of our work, none of which we feel must be specifically highlighted here.

References

- Charlotte Bunne, Ya-Ping Hsieh, Marco Cuturi, and Andreas Krause. The schrödinger bridge between gaussian measures has a closed form. In *International Conference on Artificial Intelligence and Statistics*, pp. 5802–5833. PMLR, 2023.
- Tianrong Chen, Guan-Hong Liu, and Evangelos Theodorou. Likelihood training of schrödinger bridge using forward-backward sdes theory. In *International Conference on Learning Representations*, 2021.
- Zehua Chen, Guande He, Kaiwen Zheng, Xu Tan, and Jun Zhu. Schrodinger bridges beat diffusion models on text-to-speech synthesis. *arXiv preprint arXiv:2312.03491*, 2023.
- Marco Cuturi. Sinkhorn distances: Lightspeed computation of optimal transport. *Advances in neural information processing systems*, 26, 2013.
- Marco Cuturi and Arnaud Doucet. Fast computation of Wasserstein barycenters. 2014.
- Valentin De Bortoli, James Thornton, Jeremy Heng, and Arnaud Doucet. Diffusion schrödinger bridge with applications to score-based generative modeling. *Advances in Neural Information Processing Systems*, 34:17695–17709, 2021.
- Valentin De Bortoli, Iryna Korshunova, Andriy Mnih, and Arnaud Doucet. Schrödinger bridge flow for unpaired data translation. *arXiv preprint arXiv:2409.09347*, 2024.
- Patrick Esser, Sumith Kulal, Andreas Blattmann, Rahim Entezari, Jonas Müller, Harry Saini, Yam Levi, Dominik Lorenz, Axel Sauer, Frederic Boesel, et al. Scaling rectified flow transformers for high-resolution image synthesis. *arXiv preprint arXiv:2403.03206*, 2024.
- Aude Genevay. *Entropy-regularized optimal transport for machine learning*. PhD thesis, Paris Sciences et Lettres (ComUE), 2019.
- Nikita Gushchin, Alexander Kolesov, Alexander Korotin, Dmitry Vetrov, and Evgeny Burnaev. Entropic neural optimal transport via diffusion processes. In *Advances in Neural Information Processing Systems*, 2023a.
- Nikita Gushchin, Alexander Kolesov, Petr Mokrov, Polina Karpikova, Andrey Spiridonov, Evgeny Burnaev, and Alexander Korotin. Building the bridge of schrödinger: A continuous entropic optimal transport benchmark. In *Thirty-seventh Conference on Neural Information Processing Systems Datasets and Benchmarks Track*, 2023b.
- Nikita Gushchin, Daniil Selikhanovych, Sergei Kholkin, Evgeny Burnaev, and Alexander Korotin. Adversarial schrödinger bridge matching. In *The Thirty-eighth Annual Conference on Neural Information Processing Systems*, 2024. URL <https://openreview.net/forum?id=L3Knnnigicu>.
- Jonathan Ho, Ajay Jain, and Pieter Abbeel. Denoising diffusion probabilistic models. *Advances in Neural Information Processing Systems*, 33:6840–6851, 2020.
- Ilya Igashov, Arne Schneuing, Marwin Segler, Michael M Bronstein, and Bruno Correia. Retrobridge: Modeling retrosynthesis with markov bridges. In *The Twelfth International Conference on Learning Representations*.
- Sadeep Jayasumana, Srikumar Ramalingam, Andreas Veit, Daniel Glasner, Ayan Chakrabarti, and Sanjiv Kumar. Rethinking fid: Towards a better evaluation metric for image generation. In *Proceedings of the IEEE/CVF Conference on Computer Vision and Pattern Recognition*, pp. 9307–9315, 2024.
- Mohammad Reza Karimi, Ya-Ping Hsieh, and Andreas Krause. Sinkhorn flow as mirror flow: A continuous-time framework for generalizing the sinkhorn algorithm. In *International Conference on Artificial Intelligence and Statistics*, pp. 4186–4194. PMLR, 2024.
- Diederik P Kingma and Jimmy Ba. Adam: A method for stochastic optimization. *arXiv preprint arXiv:1412.6980*, 2014.
- Peter E. Kloeden. *Numerical solution of stochastic differential equations / Peter E. Kloeden, Eckhard Platen*. Applications of mathematics; v. 23. Springer, Berlin, 1992. ISBN 0387540628.
- Solomon Kullback. Probability densities with given marginals. *The Annals of Mathematical Statistics*, 39(4):1236–1243, 1968.
- Christian Léonard. A survey of the schrödinger problem and some of its connections with optimal transport. *arXiv preprint arXiv:1308.0215*, 2013.
- Guan-Hong Liu, Arash Vahdat, De-An Huang, Evangelos A Theodorou, Weili Nie, and Anima Anandkumar. I²sb: Image-to-image schrödinger bridge. *arXiv preprint arXiv:2302.05872*, 2023a.
- Xingchao Liu, Lemeng Wu, Mao Ye, et al. Let us build bridges: Understanding and extending diffusion generative models. In *NeurIPS 2022 Workshop on Score-Based Methods*.

- Xingchao Liu, Chengyue Gong, et al. Flow straight and fast: Learning to generate and transfer data with rectified flow. In *The Eleventh International Conference on Learning Representations*, 2022.
- Xingchao Liu, Xiwen Zhang, Jianzhu Ma, Jian Peng, et al. InstafLOW: One step is enough for high-quality diffusion-based text-to-image generation. In *The Twelfth International Conference on Learning Representations*, 2023b.
- Ziwei Liu, Ping Luo, Xiaogang Wang, and Xiaoou Tang. Deep learning face attributes in the wild. In *Proceedings of International Conference on Computer Vision (ICCV)*, December 2015.
- Jan R Magnus and Heinz Neudecker. *Matrix differential calculus with applications in statistics and econometrics*. John Wiley & Sons, 2019.
- Chenlin Meng, Yutong He, Yang Song, Jiaming Song, Jijun Wu, Jun-Yan Zhu, and Stefano Ermon. Sdedit: Guided image synthesis and editing with stochastic differential equations. *arXiv preprint arXiv:2108.01073*, 2021.
- Lars Mescheder, Andreas Geiger, and Sebastian Nowozin. Which training methods for gans do actually converge? In *International conference on machine learning*, pp. 3481–3490. PMLR, 2018.
- Stefano Peluchetti. Diffusion bridge mixture transports, schrödinger bridge problems and generative modeling. *Journal of Machine Learning Research*, 24(374):1–51, 2023a.
- Stefano Peluchetti. Non-denoising forward-time diffusions. *arXiv preprint arXiv:2312.14589*, 2023b.
- Stefano Peluchetti. Bm²: Coupled schrödinger bridge matching. *arXiv preprint arXiv:2409.09376*, 2024.
- Gabriel Peyré, Marco Cuturi, et al. Computational optimal transport. *Foundations and Trends® in Machine Learning*, 11(5-6):355–607, 2019.
- Robin Rombach, Andreas Blattmann, Dominik Lorenz, Patrick Esser, and Björn Ommer. High-resolution image synthesis with latent diffusion models. In *Proceedings of the IEEE/CVF Conference on Computer Vision and Pattern Recognition*, pp. 10684–10695, 2022.
- Olaf Ronneberger, Philipp Fischer, and Thomas Brox. U-net: Convolutional networks for biomedical image segmentation. In *Medical image computing and computer-assisted intervention—MICCAI 2015: 18th international conference, Munich, Germany, October 5-9, 2015, proceedings, part III 18*, pp. 234–241. Springer, 2015.
- Erwin Schrödinger. *Über die umkehrung der naturgesetze*. Verlag der Akademie der Wissenschaften in Kommission bei Walter De Gruyter u . . . , 1931.
- Yuyang Shi, Valentin De Bortoli, Andrew Campbell, and Arnaud Doucet. Diffusion schrödinger bridge matching. In *Thirty-seventh Conference on Neural Information Processing Systems*, 2023. URL <https://openreview.net/forum?id=qy07OHsJT5>.
- Vignesh Ram Somnath, Matteo Pariset, Ya-Ping Hsieh, Maria Rodriguez Martinez, Andreas Krause, and Charlotte Bunne. Aligned diffusion schrödinger bridges. In *Uncertainty in Artificial Intelligence*, pp. 1985–1995. PMLR, 2023.
- Jiaming Song, Chenlin Meng, and Stefano Ermon. Denoising diffusion implicit models. *arXiv preprint arXiv:2010.02502*, 2020.
- Yang Song, Jascha Sohl-Dickstein, Diederik P Kingma, Abhishek Kumar, Stefano Ermon, and Ben Poole. Score-based generative modeling through stochastic differential equations. In *International Conference on Learning Representations*.
- Alexander Y Tong, Nikolay Malkin, Kilian Fatras, Lazar Atanackovic, Yanlei Zhang, Guillaume Hugué, Guy Wolf, and Yoshua Bengio. Simulation-free schrödinger bridges via score and flow matching. In *International Conference on Artificial Intelligence and Statistics*, pp. 1279–1287. PMLR, 2024.
- Francisco Vargas, Pierre Thodoroff, Austen Lamacraft, and Neil Lawrence. Solving schrödinger bridges via maximum likelihood. *Entropy*, 23(9):1134, 2021.
- Francisco Vargas, Shreyas Padhy, Denis Blessing, and Nikolas Nüsken. Transport meets variational inference: Controlled monte carlo diffusions. In *The Twelfth International Conference on Learning Representations*, 2024. URL <https://openreview.net/forum?id=PP1rudnxiW>.
- Thomas P Wihler. On the Hölder continuity of matrix functions for normal matrices. *Journal of inequalities in pure and applied mathematics*, 10(10), 2009.
- Thomas Wolf, Lysandre Debut, Victor Sanh, Julien Chaumond, Clement Delangue, Anthony Moi, Pierric Cistac, Tim Rault, Rémi Louf, Morgan Funtowicz, et al. Transformers: State-of-the-art natural language processing. In *Proceedings of the 2020 conference on empirical methods in natural language processing: system demonstrations*, pp. 38–45, 2020.

Zhisheng Xiao, Karsten Kreis, and Arash Vahdat. Tackling the generative learning trilemma with denoising diffusion gans. In *International Conference on Learning Representations*.

Hanshu Yan, Xingchao Liu, Jiachun Pan, Jun Hao Liew, Qiang Liu, and Jiashi Feng. Perflow: Piecewise rectified flow as universal plug-and-play accelerator. *arXiv preprint arXiv:2405.07510*, 2024.

Jun-Yan Zhu, Taesung Park, Phillip Isola, and Alexei A Efros. Unpaired image-to-image translation using cycle-consistent adversarial networks. In *Proceedings of the IEEE international conference on computer vision*, pp. 2223–2232, 2017.

A. Continuous-time Schrödinger Bridge Setup

For considering the continuous version of Schrödinger Bridge we denote by $\mathcal{P}(C([0, 1]), \mathbb{R}^D)$ the set of continuous stochastic processes with time $t \in [0, 1]$, i.e., the set of distributions on continuous trajectories $f : [0, 1] \rightarrow \mathbb{R}^D$. We use dW_t to denote the differential of the standard Wiener process. We denote by $p^T \in \mathcal{P}(\mathbb{R}^{D \times (N+2)})$ the discrete process which is the finite-dimensional projection of T to time moments $0 = t_0 < t_1 < \dots < t_N < t_{N+1} = 1$.

A.1. Schrödinger Bridge (SB) Problem in continuous-time

This section covers the continuous-time formulation of SB as its IPF and IMF procedures. First, we introduce several new notations to better align the continuous version with the discrete-time version considered in the main text. Consider the Markovian process T defined by the corresponding forward or backward (time-reversed) SDEs:

$$\begin{aligned} T : dx_t &= v^+(x_t, t)dt + \sqrt{\epsilon}dW_t^+, & x_0 &\sim p_0(x_0), \\ T : dx_t &= v^-(x_t, t)dt + \sqrt{\epsilon}dW_t^-, & x_1 &\sim p_1(x_1), \end{aligned}$$

where we additionally denote by W_t^+ and W_t^- the Wiener process in forward or backward time. We say $T_{|x_0}$ and $T_{|x_1}$ denotes the conditional process of T fixing the marginals using delta functions, i.e. setting $p_0(x_0) = \delta_{x_0}(x)$ and $p_1(x_1) = \delta_{x_1}(x)$:

$$\begin{aligned} T_{|x_0} : dx_t &= v^+(x_t, t)dt + \sqrt{\epsilon}dW_t^+, & x_0 &\sim \delta_{x_0}(x), \\ T_{|x_1} : dx_t &= v^-(x_t, t)dt + \sqrt{\epsilon}dW_t^-, & x_1 &\sim \delta_{x_1}(x). \end{aligned}$$

Moreover, we use $p(x_0)T_{|x_0}$ to denote the stochastic process which starts by sampling $x_0 \sim p(x_0)$ and then moving this x_0 according the SDE given by $T_{|x_0}$, i.e., $p(x_0)T_{|x_0}$ is short for the process $\int T_{|x_0} p(x_0) dx_0$. Finally, we use the shortened notation of the process $T_{|0,1}(x_0, x_1)$ conditioned on its values at times 0 and 1, saying $p^T(x_0, x_1)T_{|0,1}(x_0, x_1) = \int T_{|0,1}(x_0, x_1) p^T(x_0, x_1) dx_0 dx_1$. This visually links the following equations with the discrete-time formulation.

Schrödinger Bridge problem. Considering the continuous case, the Schrödinger Bridge problem is stated using continuous stochastic processes instead of one with predefined timesteps. Thus, the Schrödinger Bridge problem finds the most likely in the sense of Kullback-Leibler divergence stochastic process T with respect to prior Wiener process W^ϵ , i.e.:

$$\min_{T \in \mathcal{F}(p_0, p_1)} \text{KL}(T || W^\epsilon), \quad (13)$$

where $\mathcal{F}(p_0, p_1) \subset \mathcal{P}(C([0, 1]), \mathbb{R}^D)$ is the set of all stochastic processes pinned marginal distribution p_0 and p_1 at times 0 and 1, respectively. The minimization problem (13) has a unique solution T^* which can be represented as forward or backward diffusion (Léonard, 2013):

$$\begin{aligned} T^* : dx_t &= v^{*+}(x_t, t)dt + \sqrt{\epsilon}dW_t^+, & x_0 &\sim p_0(x_0), \\ T^* : dx_t &= v^{*-}(x_t, t)dt + \sqrt{\epsilon}dW_t^-, & x_1 &\sim p_1(x_1), \end{aligned}$$

where v^{*+} and v^{*-} are the corresponding drift functions.

Static Schrödinger Bridge problem. As in discrete-time, Kullback-Leibler divergence in (13) could be decomposed as follows:

$$\text{KL}(T || W^\epsilon) = \text{KL}(p^T(x_0, x_1) || p^{W^\epsilon}(x_0, x_1)) + \int \text{KL}(T_{|x_0, x_1} || W_{|x_0, x_1}^\epsilon) dp^T(x_0, x_1). \quad (14)$$

It has been proved (Léonard, 2013) that for the solution T^* it's conditional process is given by $T_{|x_0, x_1}^* = W_{|x_0, x_1}^\epsilon$. Thus, we can set $T_{|x_0, x_1} = W_{|x_0, x_1}^\epsilon$ zeroing the second term in (14) and minimize over processes with $T_{|x_0, x_1} = W_{|x_0, x_1}^\epsilon$. This leads to the equivalent Static formulation of the Schrödinger Bridge problem:

$$\min_{q \in \Pi(p_0, p_1)} \text{KL}(q(x_0, x_1) || p^{W^\epsilon}(x_0, x_1)), \quad (15)$$

where $\Pi(p_0, p_1)$ is the set of all joint distributions with marginals p_0 and p_1 . Whether time is discrete or continuous, the decomposition of SB leads to the same static formulation, which, is closely related to Entropic OT as shown in (3).

A.2. Iterative Proportional Fitting (IPF) for continuous-time

Following the main text, we describe the IPF procedure for continuous-time setup using stochastic processes. Likewise, IPF starts with setting $T^0 = p_0(x_0)W_{|x_0}^\epsilon$ and then it alternates between following projections:

$$T^{2k+1} = \text{proj}_1 \left(p^{T^{2k}}(x_1)T_{|x_1}^{2k} \right) \stackrel{\text{def}}{=} p_1(x_1)T_{|x_1}^{2k}, \quad (16)$$

$$T^{2k+2} = \text{proj}_0 \left(p^{T^{2k+1}}(x_0)T_{|x_0}^{2k+1} \right) \stackrel{\text{def}}{=} p_0(x_0)T_{|x_0}^{2k+1}. \quad (17)$$

As in the discrete-time case, these projections replace marginal distributions $p^T(x_1)$ and $p^T(x_0)$ in the processes $p^T(x_1)T_{|x_1}$ and $p^T(x_0)T_{|x_0}$ by $p_1(x_1)$ and $p_0(x_0)$ respectively. Similarly to discrete-time formulation, the sequence of T^k converges to the solution of the Schrödinger Bridge problem T^* implicitly the reverse Kullback-Leibler divergence $\text{KL}(T^k||T^*)$ between the current process T^k and the solution to the SB problem T^* . Additionally, it should be mentioned that projections are conducted by numerical approximation of forward and time-reversed conditional processes, $T_{|x_0}$ and $T_{|x_1}$, by learning their drifts via one of the methods: score matching (De Bortoli et al., 2021) or maximum likelihood estimation (Vargas et al., 2021).

A.3. Iterative Markovian Fitting (IMF) for continuous-time

IMF introduces new projections that alternate between reciprocal and Markovian processes starting from any process T^0 pinned by p_0 and p_1 , i.e. in $\mathcal{F}(p_0, p_1)$:

$$T^{2k+1} = \text{proj}_{\mathcal{R}} (T^{2k}) \stackrel{\text{def}}{=} p^{T^{2k}}(x_0, x_1)W_{|x_0, x_1}^\epsilon, \quad (18)$$

$$T^{2k+2} = \text{proj}_{\mathcal{M}} (T^{2k+1}) \stackrel{\text{def}}{=} \underbrace{p^{T^{2k+1}}(x_0)T_{M|x_0}^{2k+1}}_{\text{forward representation}} = \underbrace{p^{T^{2k+1}}(x_1)T_{M|x_1}^{2k+1}}_{\text{backward representation}}. \quad (19)$$

where we denote by T_M the Markovian projections of the processes T , which can be represented as the forward or backward time diffusion as follows (Gushchin et al., 2024, Section 2.1):

$$T_M : dx_t^+ = v_M^+(x_t^+, t)dt + \sqrt{\epsilon}dW_t^+, \quad x_0 \sim p^T(x_0), \quad v_M^+(x_t^+, t) = \int \frac{x_1 - x_t^+}{1-t} p^T(x_1|x_t)dx_1,$$

$$T_M : dx_t^- = v_M^-(x_t^-, t)dt + \sqrt{\epsilon}dW_t^-, \quad x_1 \sim p^T(x_1), \quad v_M^-(x_t^-, t) = \int \frac{x_0 - x_t^-}{1-t} p^T(x_0|x_t)dx_0.$$

This procedure converges to a unique solution, which is the Schrödinger bridge T^* (Léonard, 2013). While reciprocal projection can be easily done by combining the joint distribution $p^T(x_0, x_1)$ of the process T and Brownian bridge $W_{|x_0, x_1}^\epsilon$, the Markovian projection is much more challenging and must be fitted via Bridge matching (Shi et al., 2023; Liu et al.; Peluchetti, 2023b).

Since the result of the Markovian projection can be represented (7) both by forward and backward representation, in practice, neural networks v_θ^+ (**forward parametrization**) or v_ϕ^- (**backward parametrization**) are used to learn the corresponding drifts of the Markovian projections. In turn, starting distributions are set to be $p_0(x_0)$ for forward parametrization and $p_1(x_1)$ for the backward parametrization. So, this **bidirectional** procedure can be described as follows:

$$T^{4k+1} = \underbrace{p^{T^{4k}}(x_0, x_1)W_{|x_0, x_1}^\epsilon}_{\text{proj}_{\mathcal{R}}(T^{4k})}, \quad T^{4k+2} = \underbrace{p_1(x_1)T_{M|x_1}^{4k+1}}_{\text{backward parametrization}}, \quad (20)$$

$$T^{4k+3} = \underbrace{p^{T^{4k+2}}(x_0, x_1)W_{|x_0, x_1}^\epsilon}_{\text{proj}_{\mathcal{R}}(T^{4k+2})}, \quad T^{4k+4} = \underbrace{p_0(x_0)T_{M|x_0}^{4k+3}}_{\text{forward parametrization}}. \quad (21)$$

A.4. Iterative Proportional Markovian Fitting (IPMF) for continuous-time

Here, we analyze the continuous version of the heuristical bidirectional IMF. First, we recall, that the IPF projections $\text{proj}_0(T)$ and $\text{proj}_1(T)$ given by (16) and (17) of the Markovian process T is just change the starting distribution from $p^T(x_0)$ to $p_0(x_0)$ and $p^T(x_1)$ to $p_1(x_1)$.

Now we note that the process T^{4k+2} in (20) is obtained by using a combination of Markovian projection $\text{proj}_{\mathcal{M}}$ given by (19) in forward parametrization and IPF projection proj_1 given by (17):

$$T^{4k+2} = p_1(x_1)T_{M|x_1}^{4k+1} = \underbrace{\text{proj}_1(p^{T^{4k+1}}(x_1)T_{M|x_1}^{4k+1})}_{\text{proj}_1(\text{proj}_{\mathcal{M}}(T^{4k+1}))}.$$

In turn, the process T^{4k+4} in (21) is obtained by using a combination of Markovian projection $\text{proj}_{\mathcal{M}}$ given by (19) in backward parametrization and IPF projection proj_0 given by (16):

$$T^{4k+4} = p_0(x_0)T_{M|x_0}^{4k+3} = \underbrace{\text{proj}_0(p^{T^{4k+3}}(x_0)T_{M|x_0}^{4k+3})}_{\text{proj}_0(\text{proj}_{\mathcal{M}}(T^{4k+3}))}.$$

Combining these facts we can rewrite bidirectional IMF in the following manner:

Iterative Proportional Markovian Fitting (Conitnious time setting)

$$T^{4k+1} = \underbrace{p^{T^{4k}}(x_0, x_1)W_{|x_0, x_1}^\epsilon}_{\text{proj}_{\mathcal{R}}(T^{4k})}, \quad T^{4k+2} = \underbrace{p_1(x_1)T_{M|x_1}^{4k+1}}_{\text{proj}_1(\text{proj}_{\mathcal{M}}(T^{4k+1}))} \quad (22)$$

$$T^{4k+3} = \underbrace{p^{T^{4k+2}}(x_0, x_1)W_{|x_0, x_1}^\epsilon}_{\text{proj}_{\mathcal{R}}(T^{4k+2})}, \quad T^{4k+4} = \underbrace{p_0(x_0)T_{M|x_0}^{4k+3}}_{\text{proj}_0(\text{proj}_{\mathcal{M}}(T^{4k+3}))}. \quad (23)$$

Thus, we obtain the analog of the discrete-time IPMF procedure, which concludes our description of the continuous setups.

B. Theoretical Analysis for Gaussians

Here, we study behavior of IPMF with volatility ϵ between D -dimensional Gaussians $p_0 = \mathcal{N}(\mu_0, \Sigma_0)$ and $p_1 = \mathcal{N}(\mu_1, \Sigma_1)$. For convenience, we use notation ϵ_* instead of ϵ . For various settings, we prove that the parameters of q^{4k} with each step exponentially converge to desired values $\mu_0, \mu_1, \Sigma_0, \Sigma_1, \epsilon_*$. The steps are as follows:

- 1) In Appendix B.1, we reveal the connection between $2D$ -dimensional Gaussian distribution and solution of entropic OT problem with specific transport cost, i.e., we prove our Lemma 3.1.
- 2) In Appendix B.2, we study the effect of IPF steps on the current process. We show that during these steps, the marginals become close to p_0 and p_1 , and the optimality matrix does not change. We also prove that the spectral norms of the marginal matrices are bounded during the whole IPMF procedure.
- 3) In Appendix B.3, we study the effect of IMF step on the current process when $D > 1$. We show that after DIMF step with $N = 1$, the distance between current optimality matrix and desired one can be bounded by the scaled previous distance. We also derive conditions of ϵ under which the scale factor is contractive.
- 4) In Appendix B.4, we study the effect of IMF step in a particular case $D = 1$. We show that after IMF (continuous or discrete with $N = 1$), marginals remain the same, and the new correlation becomes close to the correlation of the static ϵ_* -EOT solution between marginals.
- 5) Finally, in Appendices B.5 and B.6, we prove our main Theorem 3.2 for the case $D > 1$ and $D = 1$, respectively.

B.1. Gaussian plans as entropic optimal transport plans

Proof of Lemma 3.1. We note that we can add any functions $f(x_0)$ and $g(x_1)$ depending only on x_0 or x_1 , respectively, to the cost function $c_A(x_0, x_1) = x_1^\top A x_0$, and the OT solution will not change. This is because the integrals of such functions over any transport plan will be constants, as they will depend only on the marginals (which are given) but not on the plan itself. Thus, for any $A \in \mathbb{R}^{D \times D}$, we can rearrange the cost term $c_A(x_0, x_1)$ so that it becomes lower-bounded:

$$\tilde{c}_A(x_0, x_1) = \|Ax_0\|^2/2 - x_1^\top Ax_0 + \|x_1\|^2/2 = \|Ax_0 - x_1\|^2/2 \geq 0,$$

where $\tilde{c}_A(x_0, x_1)$ is a lower bounded function. Following (Gushchin et al., 2023b, Theorem 3.2), the conditional distribution $q_c(x_1|x_0)$ with the lower bounded cost function c_A can be expressed as:

$$q_{c_A}(x_0|x_1) \propto \exp(-c_A(x_0, x_1) + f_{c_A}(x_0)) = \exp(x_1^\top Ax_0 + f_{c_A}(x_0)),$$

where function $f_{c_A}(x_1)$ depends only on x_1 . Moreover, we can simplify this distribution to

$$q_{c_A}(x_0|x_1) = Z_{x_0} Z_{x_1} \exp(x_1^\top A x_0), \quad (24)$$

where factors Z_{x_0} and Z_{x_1} depend only on x_0 and x_1 , respectively. Meanwhile, the conditional distribution of $q(x_0|x_1)$ has a closed form, namely,

$$\begin{aligned} q(x_0|x_1) &= \mathcal{N}\left(x_0 | \tilde{\mu} + P(\tilde{\Sigma})^{-1}(x_1 - \tilde{\mu}), \Sigma - P(\tilde{\Sigma})^{-1}P^\top\right) \\ &= Z_{x_0} Z_{x_1} \exp\left(x_0^\top (\Sigma - P(\tilde{\Sigma})^{-1}P^\top)^{-1} P(\tilde{\Sigma})^{-1} x_1\right). \end{aligned}$$

where factors Z_{x_0} and Z_{x_1} depend only on x_0 and x_1 , respectively. Equating terms of $q(x_0|x_1)$ and $q_{c_A}(x_0|x_1)$ which depend on x_0 and x_1 simultaneously, we obtain the required function

$$A = (\tilde{\Sigma})^{-1}P^\top(\Sigma - P(\tilde{\Sigma})^{-1}P^\top)^{-1}, \quad (25)$$

which concludes that q solves 1-entropic OT with the cost function $-x_0^\top A x_1$. \square

B.2. IPF step analysis

We use IPMF with parameter ϵ_* between distributions $\mathcal{N}(\mu_0, \Sigma_0)$ and $\mathcal{N}(\mu_1, \Sigma_1)$. We start with the process $\mathcal{N}\left(\begin{pmatrix} \mu_0 \\ \nu \end{pmatrix}, \begin{pmatrix} \Sigma_0 & P \\ P & S \end{pmatrix}\right)$ with correlation P .

Recall that one IPMF step consists of 4 consecutive steps:

1. IMF step refining current optimality value,
2. IPF step changing final prior to $\mathcal{N}(\mu_1, \Sigma_1)$,
3. IMF step refining current optimality value,
4. IPF step changing starting prior to $\mathcal{N}(\mu_0, \Sigma_0)$.

We use the following notations for the covariance matrices changes during IPMF step:

$$\begin{aligned} \begin{pmatrix} \Sigma_0 & P \\ P^\top & S \end{pmatrix} &\xrightarrow{\text{IMF}} \begin{pmatrix} \Sigma_0 & \tilde{P} \\ \tilde{P}^\top & S \end{pmatrix} \xrightarrow{\text{IPF}} \begin{pmatrix} (S') & P' \\ (P')^\top & \Sigma_1 \end{pmatrix} \\ &\xrightarrow{\text{IMF}} \begin{pmatrix} S' & \hat{P} \\ \hat{P}^\top & \Sigma_1 \end{pmatrix} \xrightarrow{\text{IPF}} \begin{pmatrix} \Sigma_0 & P'' \\ (P'')^\top & S'' \end{pmatrix}, \end{aligned}$$

and for the means the changes are:

$$\begin{pmatrix} \mu_0 \\ \nu \end{pmatrix} \xrightarrow{\text{IMF}} \begin{pmatrix} \mu_0 \\ \nu \end{pmatrix} \xrightarrow{\text{IPF}} \begin{pmatrix} \nu' \\ \mu_1 \end{pmatrix} \xrightarrow{\text{IMF}} \begin{pmatrix} \nu' \\ \mu_1 \end{pmatrix} \xrightarrow{\text{IPF}} \begin{pmatrix} \mu_0 \\ \nu'' \end{pmatrix}.$$

Lemma B.1 (Improvement after IPF steps). *Consider an initial 2D-dimensional Gaussian joint distribution $\mathcal{N}\left(\begin{pmatrix} \mu_0 \\ \nu \end{pmatrix}, \begin{pmatrix} \Sigma_0 & P \\ P^\top & S \end{pmatrix}\right) \in \mathcal{P}_{2,ac}(\mathbb{R}^D \times \mathbb{R}^D)$. We run IPMF step between distributions $\mathcal{N}(\mu_0, \Sigma_0)$ and $\mathcal{N}(\mu_1, \Sigma_1)$ and obtain new joint distribution $\mathcal{N}\left(\begin{pmatrix} \mu_0 \\ \mu'' \end{pmatrix}, \begin{pmatrix} \Sigma_0 & P'' \\ (P'')^\top & S'' \end{pmatrix}\right)$. Then, the distance between ground truth μ_1, Σ_1 and the new joint distribution parameters decreases as:*

$$\|(S'')^{-\frac{1}{2}}\Sigma_1(S'')^{-\frac{1}{2}} - I_D\|_2 \leq \|\tilde{P}_n\|_2^2 \cdot \|P''_n\|_2^2 \cdot \|S^{-\frac{1}{2}}\Sigma_1 S^{-\frac{1}{2}} - I_D\|_2, \quad (26)$$

$$\|\Sigma_1^{-\frac{1}{2}}(\nu'' - \mu_1)\|_2 \leq \|\hat{P}_n\|_2 \cdot \|P''_n\|_2 \cdot \|\Sigma_1^{-\frac{1}{2}}(\nu - \mu_1)\|_2, \quad (27)$$

where $\tilde{P}_n := \Sigma_0^{-1/2} \tilde{P} S^{-1/2}$, $P''_n := (S')^{-\frac{1}{2}} P' \Sigma_1^{-\frac{1}{2}}$, $\hat{P}_n := (S')^{-1/2} \hat{P} \Sigma_1^{-1/2}$ and $P''_n := \Sigma_0^{-1/2} P'' (S'')^{-1/2}$ are normalized matrices whose spectral norms are not greater than 1.

Proof. During IPF steps, we keep the conditional distribution and change the marginal. For the first IPF, we keep the inner part $x_0|x_1$ for all $x_1 \in \mathbb{R}^D$:

$$\mathcal{N}\left(x_0|\mu_0 + \tilde{P}S^{-1}(x_1 - \nu), \Sigma_0 - \tilde{P}S^{-1}\tilde{P}^\top\right) = \mathcal{N}\left(x_0|\nu' + P'\Sigma_1^{-1}(x_1 - \mu_1), S' - P'\Sigma_1^{-1}(P')^\top\right).$$

This is equivalent to the system of equations:

$$\Sigma_0 - \tilde{P}S^{-1}\tilde{P}^\top = S' - P'\Sigma_1^{-1}(P')^\top, \quad (28)$$

$$P'\Sigma_1^{-1} = \tilde{P}S^{-1}, \quad (29)$$

$$\mu_0 - \tilde{P}S^{-1}\nu = \nu' - P'\Sigma_1^{-1}\mu_1. \quad (30)$$

Similarly, after the second IPF step, we have equations:

$$\Sigma_1 - \hat{P}^\top(S')^{-1}\hat{P} = S'' - (P'')^\top\Sigma_0^{-1}P'', \quad (31)$$

$$(P'')^\top\Sigma_0^{-1} = \hat{P}^\top(S')^{-1}, \quad (32)$$

$$\mu_1 - \hat{P}^\top(S')^{-1}\nu' = \nu'' - (P'')^\top\Sigma_0^{-1}\mu_0. \quad (33)$$

Covariance matrices. Combining equations (29), (28) and (32), (31) together, we obtain:

$$\Sigma_0 - S' = \tilde{P}S^{-1}(S - \Sigma_1)S^{-1}\tilde{P}^\top, \quad //(32), (31) \quad (34)$$

$$I_D - \Sigma_0(S')^{-1} = \tilde{P}S^{-1}(\Sigma_1 - S)S^{-1}\tilde{P}^\top(S')^{-1}, \quad //(34) \cdot (S')^{-1} \quad (35)$$

$$\Sigma_1 - S'' = \hat{P}^\top(S')^{-1}(I_D - \Sigma_0(S')^{-1})\hat{P}, \quad //(29), (28) \quad (36)$$

$$\Sigma_1 - S'' = \hat{P}^\top(S')^{-1}\tilde{P}S^{-1}(\Sigma_1 - S)S^{-1}\tilde{P}^\top(S')^{-1}\hat{P}, \quad //(35) \text{ insert to } (36)$$

$$\Sigma_1 - S'' = (P'')^\top\Sigma_0^{-1}\tilde{P}S^{-1}(\Sigma_1 - S)S^{-1}\tilde{P}^\top\Sigma_0^{-1}P'', \quad //change using (32)$$

$$(S'')^{-\frac{1}{2}}\Sigma_1(S'')^{-\frac{1}{2}} - I_D = (S'')^{-\frac{1}{2}}(P'')^\top\Sigma_0^{-\frac{1}{2}} \cdot \Sigma_0^{-\frac{1}{2}}\tilde{P}S^{-\frac{1}{2}} \cdot (S^{-\frac{1}{2}}\Sigma_1S^{-\frac{1}{2}} - I_D) \cdot S^{-\frac{1}{2}}\tilde{P}^\top\Sigma_0^{-\frac{1}{2}} \cdot \Sigma_0^{-\frac{1}{2}}P''(S'')^{-\frac{1}{2}}.$$

The matrices (28) and (31) must be SPD to be covariance matrices:

$$\Sigma_0 - \tilde{P}S^{-1}\tilde{P}^\top \succeq 0 \quad \implies \quad I_D \succeq \Sigma_0^{-1/2}\tilde{P}S^{-1/2} \cdot S^{-1/2}\tilde{P}^\top\Sigma_0^{-1/2},$$

$$S'' - (P'')^\top\Sigma_0^{-1}P'' \succeq 0 \quad \implies \quad I_D \succeq \Sigma_0^{-1/2}P''(S'')^{-1/2} \cdot (S'')^{-1/2}(P'')^\top\Sigma_0^{-1/2}.$$

In other words, denoting matrices $\tilde{P}_n := \Sigma_0^{-1/2}\tilde{P}S^{-1/2}$ and $P''_n := \Sigma_0^{-1/2}P''(S'')^{-1/2}$, we can bound their spectral norms as $\|\tilde{P}_n\|_2 \leq 1$ and $\|P''_n\|_2 \leq 1$. We write down the final transaction for covariance matrices:

$$(S'')^{-\frac{1}{2}}\Sigma_1(S'')^{-\frac{1}{2}} - I_D = (P''_n)^\top \cdot \tilde{P}_n \cdot (S^{-\frac{1}{2}}\Sigma_1S^{-\frac{1}{2}} - I_D) \cdot \tilde{P}_n^\top \cdot P''_n. \quad (37)$$

Hence, the spectral norm of the difference between ground truth Σ_1 and current S'' drops exponentially as:

$$\|(S'')^{-\frac{1}{2}}\Sigma_1(S'')^{-\frac{1}{2}} - I_D\|_2 \leq \|\tilde{P}_n\|_2^2 \cdot \|P''_n\|_2^2 \cdot \|S^{-\frac{1}{2}}\Sigma_1S^{-\frac{1}{2}} - I_D\|_2.$$

Means. Combining equations (30), (29) and (33), (32) together, we obtain:

$$\mu_0 - \nu' = \tilde{P}S^{-1}\nu - P'\Sigma_1^{-1}\mu_1 = P'\Sigma_1^{-1}(\nu - \mu_1), \quad //(30), (29) \quad (38)$$

$$\nu'' - \mu_1 = (P'')^\top\Sigma_0^{-1}\mu_0 - \hat{P}^\top(S')^{-1}\nu' = \hat{P}^\top(S')^{-1}(\mu_0 - \nu'), \quad //(33), (32) \quad (39)$$

$$\nu'' - \mu_1 = \hat{P}^\top(S')^{-1}P'\Sigma_1^{-1}(\nu - \mu_1), \quad //insert (38) to (39)$$

$$\Sigma_1^{-\frac{1}{2}}(\nu'' - \mu_1) = \Sigma_1^{-\frac{1}{2}}\hat{P}^\top(S')^{-\frac{1}{2}} \cdot (S')^{-\frac{1}{2}}P'\Sigma_1^{-\frac{1}{2}} \cdot \Sigma_1^{-\frac{1}{2}}(\nu - \mu_1).$$

The matrices (28) and (31) must be SPD to be covariance matrices:

$$S' - P'\Sigma_1^{-1}(P')^\top \succeq 0 \quad \implies \quad I_D \succeq (S')^{-\frac{1}{2}}P'\Sigma_1^{-\frac{1}{2}} \cdot \Sigma_1^{-\frac{1}{2}}(P')^\top(S')^{-\frac{1}{2}},$$

$$\Sigma_1 - \hat{P}^\top(S')^{-1}\hat{P} \succeq 0 \quad \implies \quad I_D \succeq \Sigma_1^{-1/2}\hat{P}^\top(S')^{-1/2} \cdot (S')^{-1/2}\hat{P}\Sigma_1^{-1/2}.$$

Denoting matrices $P'_n := (S')^{-\frac{1}{2}} P' \Sigma_1^{-\frac{1}{2}}$ and $\hat{P}_n := (S')^{-1/2} \hat{P} \Sigma_1^{-1/2}$, we can bound their spectral norms as $\|P'_n\|_2 \leq 1$ and $\|\hat{P}_n\|_2 \leq 1$. We use this to estimate the ℓ_2 -norm of the difference between the ground truth μ_1 and the current mean:

$$\begin{aligned} \Sigma_1^{-\frac{1}{2}}(\nu'' - \mu_1) &= \hat{P}_n^\top \cdot P'_n \cdot \Sigma_1^{-\frac{1}{2}}(\nu - \mu_1), \\ \|\Sigma_1^{-\frac{1}{2}}(\nu'' - \mu_1)\|_2 &\leq \|\hat{P}_n^\top\|_2 \cdot \|P'_n\|_2 \cdot \|\Sigma_1^{-\frac{1}{2}}(\nu - \mu_1)\|_2. \end{aligned} \quad (40)$$

□

Lemma B.2 (Marginals norm bound during IPMF procedure). *Consider an initial 2D-dimensional Gaussian joint distribution $\mathcal{N}\left(\begin{pmatrix} \mu_0 \\ \nu_0 \end{pmatrix}, \begin{pmatrix} \Sigma_0 & P_0 \\ P_0^\top & S \end{pmatrix}\right) \in \mathcal{P}_{2,ac}(\mathbb{R}^D \times \mathbb{R}^D)$. We run k IPMF step between distributions $\mathcal{N}(\mu_0, \Sigma_0)$ and $\mathcal{N}(\mu_1, \Sigma_1)$ and obtain new joint distribution $\mathcal{N}\left(\begin{pmatrix} \mu_0 \\ \nu_k \end{pmatrix}, \begin{pmatrix} \Sigma_0 & P_k \\ P_k^\top & S_k \end{pmatrix}\right)$. Then the norm $\|S_k\|$ can be bounded independently of k by:*

$$\|S_k\|_2 \leq \frac{\|\Sigma_1\|_2}{\min\{\lambda_{\min}(S_0^{-\frac{1}{2}} \Sigma_1 S_0^{-\frac{1}{2}}), 1\}}, \quad \|S_k^{-1}\|_2 \leq \max\{\lambda_{\max}(S_0^{-\frac{1}{2}} \Sigma_1 S_0^{-\frac{1}{2}}), 1\} \|\Sigma_1^{-1}\|_2. \quad (41)$$

Proof. Consider the last IPMF step. We denote symmetric matrices $\Delta_k := S_k^{-\frac{1}{2}} \Sigma_1 S_k^{-\frac{1}{2}} - I_D$, $\Delta_{k-1} := S_{k-1}^{-\frac{1}{2}} \Sigma_1 S_{k-1}^{-\frac{1}{2}} - I_D$ and $\hat{\lambda}_{\min}(\Delta) := \min\{0, \lambda_{\min}(\Delta)\}$, $\hat{\lambda}_{\max}(\Delta) := \max\{0, \lambda_{\max}(\Delta)\}$. Next, we estimate spectral norm of S_{k-1} as follows:

$$\begin{aligned} \Delta_k = S_k^{-\frac{1}{2}} \Sigma_1 S_k^{-\frac{1}{2}} - I_D &\succeq \lambda_{\min}(\Delta_k) I_D \succeq \hat{\lambda}_{\min}(\Delta_k) I_D, \\ S_k^{-\frac{1}{2}} \Sigma_1 S_k^{-\frac{1}{2}} &\succeq (\hat{\lambda}_{\min}(\Delta_k) + 1) I_D, \\ \Sigma_1 &\succeq (\hat{\lambda}_{\min}(\Delta_k) + 1) S_k \end{aligned}$$

Note, that by design we have $\Delta_k \succeq -I_D \Rightarrow -1 \leq \hat{\lambda}_{\min}(\Delta_k) \leq 0 \Rightarrow 0 \leq (\hat{\lambda}_{\min}(\Delta_k) + 1) \leq 1$ and can obtain

$$\begin{aligned} \Sigma_1 &\succeq (\hat{\lambda}_{\min}(\Delta_k) + 1) S_k, \\ S_k &\preceq \frac{1}{\hat{\lambda}_{\min}(\Delta_k) + 1} \Sigma_1, \\ \|S_k\|_2 &\leq \frac{\|\Sigma_1\|_2}{\hat{\lambda}_{\min}(\Delta_k) + 1}. \end{aligned} \quad (42)$$

Similarly, we prove that

$$S_k \succeq \frac{1}{\hat{\lambda}_{\max}(\Delta_k) + 1} \Sigma_1 \Rightarrow \|S_k^{-1}\|_2 \leq (\hat{\lambda}_{\max}(\Delta_k) + 1) \|\Sigma_1^{-1}\|_2.$$

Now, we prove that $\hat{\lambda}_{\min}(\Delta_k) \geq \hat{\lambda}_{\min}(\Delta_{k-1})$. We denote by P''_n and \tilde{P}_n normalized matrices after the second IPF step and the first IMF step on the last iteration, respectively (see Lemma B.1). For any $x \in \mathbb{R}^D$, $\|x\|_2 \leq 1$, we calculate the bilinear form:

$$\begin{aligned} x^\top \Delta_k x &\stackrel{(37)}{=} x^\top (P''_n)^\top \cdot \tilde{P}_n \cdot (S_{k-1}^{-\frac{1}{2}} \Sigma_1 S_{k-1}^{-\frac{1}{2}} - I_D) \cdot \tilde{P}_n^\top \cdot P''_n x = (\tilde{P}_n^\top \cdot P''_n x)^\top \Delta_{k-1} (\tilde{P}_n^\top \cdot P''_n x), \\ \hat{\lambda}_{\min}(\Delta_k) &= \min \left\{ 0, \min_{\|x\|_2 \leq 1} x^\top \Delta_k x \right\} \geq \min \left\{ 0, \min_{\|x\|_2 \leq 1} (\tilde{P}_n^\top \cdot P''_n x)^\top \Delta_{k-1} (\tilde{P}_n^\top \cdot P''_n x) \right\} \\ &\geq \min \left\{ 0, \min_{\|x\|_2 \leq 1} (\tilde{P}_n^\top \cdot P''_n x)^\top \Delta_{k-1} (\tilde{P}_n^\top \cdot P''_n x) \right\} \\ &\geq \|\tilde{P}_n^\top \cdot P''_n x\|_2^2 \cdot \min \{0, \lambda_{\min}(\Delta_{k-1})\} \geq \|\tilde{P}_n\|^2 \|P''_n\|^2 \|x\|_2^2 \cdot \hat{\lambda}_{\min}(\Delta_{k-1}) \geq \hat{\lambda}_{\min}(\Delta_{k-1}). \end{aligned}$$

Hence, after each IPMF step $\hat{\lambda}_{\min}(\Delta_k)$ decreases and can be upper bounded by the initial value $\hat{\lambda}_{\min}(\Delta_k) \geq \hat{\lambda}_{\min}(\Delta_0)$ using math induction. It implies that, for all steps, norms are bounded by

$$\|S_k\|_2 \stackrel{(42)}{\leq} \frac{\|\Sigma_1\|_2}{\hat{\lambda}_{\min}(\Delta_k) + 1} \leq \frac{\|\Sigma_1\|_2}{\hat{\lambda}_{\min}(\Delta_0) + 1} = \frac{\|\Sigma_1\|_2}{\min\{\lambda_{\min}(S_0^{-\frac{1}{2}} \Sigma_1 S_0^{-\frac{1}{2}}), 1\}}.$$

Similarly, we prove that

$$\hat{\lambda}_{max}(\Delta_k) \leq \hat{\lambda}_{max}(\Delta_{k-1}) \Rightarrow \|S_k^{-1}\|_2 \leq (\hat{\lambda}_{max}(\Delta_0) + 1)\|\Sigma_1^{-1}\|_2 \leq \max\{\lambda_{max}(S_0^{-\frac{1}{2}}\Sigma_1 S_0^{-\frac{1}{2}}), 1\}\|\Sigma_1^{-1}\|_2.$$

□

Lemma B.3 (IPF step does not change optimality matrix A). *Consider an initial 2D-dimensional Gaussian joint distribution $\mathcal{N}\left(\begin{pmatrix} \mu_0 \\ \nu \end{pmatrix}, \begin{pmatrix} \Sigma_0 & P \\ P^\top & S \end{pmatrix}\right) \in \mathcal{P}_{2,ac}(\mathbb{R}^D \times \mathbb{R}^D)$. We run IPF step between distributions $\mathcal{N}(\mu_0, \Sigma_0)$ and $\mathcal{N}(\mu_1, \Sigma_1)$ and obtain new joint distribution $\mathcal{N}\left(\begin{pmatrix} \nu' \\ \mu_1 \end{pmatrix}, \begin{pmatrix} S' & P' \\ P' & \Sigma_1 \end{pmatrix}\right)$. Then, IPF step does not change optimality matrix A , i.e.,*

$$A = \Xi(P, \Sigma_0, S) = \Xi(P', S', \Sigma_1).$$

Proof. The explicit formulas for $\Xi(\tilde{P}, \Sigma_0, S)$ and $\Xi(P', S', \Sigma_1)$ are

$$\begin{aligned} \Xi(P, \Sigma_0, S) &= S^{-1}P^\top \cdot (\Sigma_0 - \tilde{P}S^{-1}P^\top), \\ \Xi(P', S', \Sigma_1) &= \Sigma_1^{-1}(P')^\top \cdot (S' - P'\Sigma_1^{-1}(P')^\top). \end{aligned}$$

The first terms are equal due to equation (29), and the second terms are equal due to (28).

We can prove this lemma in more general way. We derive the formula (25) for A only from the shape of the conditional distribution $q(x_0|x_1)$ (24). During IPF step, this distribution remains the same by design, while parameters S, \tilde{P} change. Hence, IPF step has no effect on the optimality matrix. □

B.3. IMF step analysis: multidimensional case for large ϵ

Lemma B.4 (IMF step). *Let $Q, S \succ 0$ and define on the ball $\{P : \|P\|_2 \leq 1\}$ a function*

$$f(P) = (Q + PS^{1/2}) \left(Q + S + Q^{1/2}PS^{1/2} + (Q^{1/2}PS^{1/2})^\top + \epsilon I \right)^{-1} (S^{1/2} + Q^{1/2}P).$$

Then $f(P)$ is Lipschitz continuous with constant

$$\gamma(\epsilon, \|Q\|_2, \|S\|_2) = \frac{\left(\|Q\|_2^{1/2} + \|S\|_2^{1/2}\right)^2}{\epsilon} + \frac{2}{\epsilon^2} \|Q\|_2^{1/2} \|S\|_2^{1/2} \left(\|S\|_2^{1/2} + \|Q\|_2^{1/2}\right)^2. \quad (43)$$

Moreover,

$$\|f(P)\|_2 \leq \frac{2\|Q\|_2 + 2\|S\|_2}{\epsilon + 2\|Q\|_2 + 2\|S\|_2}. \quad (44)$$

Proof. IMF step yields new P' such that

$$f(P) = P' = (Q^{1/2} + PS^{1/2}) \left(Q + S + Q^{1/2}PS^{1/2} + (Q^{1/2}PS^{1/2})^\top + \epsilon I \right)^{-1} (S^{1/2} + Q^{1/2}P).$$

Let $\tilde{R}_p = Q + S + Q^{1/2}PS^{1/2} + (Q^{1/2}PS^{1/2})^\top + \epsilon I$. Differentiating by P yields

$$\begin{aligned} dP' &= dPS^{1/2}\tilde{R}_p^{-1} \left(S^{1/2} + Q^{1/2}P \right) + \left(Q^{1/2} + PS^{1/2} \right) \tilde{R}_p^{-1} Q^{1/2} dP \\ &\quad - \left(Q^{1/2} + PS^{1/2} \right) \tilde{R}_p^{-1} \left(Q^{1/2} dPS^{1/2} + (Q^{1/2} dPS^{1/2})^\top \right) \tilde{R}_p^{-1} \left(S^{1/2} + Q^{1/2}P \right). \end{aligned}$$

Since $\tilde{R}_p \succ \epsilon I$, we get

$$\|dP'\|_2 \leq \|dP\|_2 \left(\frac{\left(\|Q^{1/2}\|_2 + \|S^{1/2}\|_2\right)^2}{\epsilon} + \frac{2}{\epsilon^2} \|Q^{1/2}\|_2 \|S^{1/2}\|_2 \left(\|S^{1/2}\|_2 + \|Q^{1/2}\|_2\right)^2 \right)$$

This yields

$$\|df(P)\|_2 \leq \gamma(\epsilon, \|S\|_2, \|Q\|_2) \|dP\|_2$$

Now we prove (44). Consider

$$P'(P')^\top = (Q^{1/2} + PS^{1/2})\tilde{R}_p^{-1}(S^{1/2} + Q^{1/2}P)(S^{1/2} + P^\top Q^{1/2})\tilde{R}_p^{-1}(Q^{1/2} + S^{1/2}P^\top). \quad (45)$$

Now, recall that $I - PP^\top \succcurlyeq 0$

$$(S^{1/2} + Q^{1/2}P)(S^{1/2} + P^\top Q^{1/2}) = \tilde{R}_p - \epsilon I - Q^{1/2}(I - P(P)^\top) \preccurlyeq \tilde{R}_p - \epsilon I.$$

Thus, (45) can be continued as

$$\begin{aligned} P'(P')^\top &\preccurlyeq (Q^{1/2} + PS^{1/2})\tilde{R}_p^{-1}(\tilde{R}_p - \epsilon I)\tilde{R}_p^{-1}(Q^{1/2} + S^{1/2}P^\top) \\ &= (Q^{1/2} + PS^{1/2})\tilde{R}_p^{-1/2}(I - \epsilon\tilde{R}_p^{-1})\tilde{R}_p^{-1/2}(Q^{1/2} + S^{1/2}P^\top) \\ &\preccurlyeq \left(1 - \epsilon\lambda_{\min}(\tilde{R}_p^{-1})\right)(Q^{1/2} + PS^{1/2})\tilde{R}_p^{-1}(Q^{1/2} + S^{1/2}P^\top). \end{aligned}$$

Next, we consider

$$\begin{aligned} \|(Q^{1/2} + PS^{1/2})\tilde{R}_p^{-1}(Q^{1/2} + S^{1/2}P^\top)\|_2 &= \|(Q^{1/2} + PS^{1/2})\tilde{R}_p^{-1/2}\|_2^2 \\ &= \|\tilde{R}_p^{-1/2}(Q^{1/2} + S^{1/2}P^\top)(Q^{1/2} + PS^{1/2})\tilde{R}_p^{-1/2}\|_2 = \|\tilde{R}_p^{-1/2}(Q + P + P^\top + S^{1/2}(P')^\top P'S^{1/2})\tilde{R}_p^{-1/2}\|_2 \\ &= \|\tilde{R}_p^{-1/2}(\tilde{R}_p - \epsilon I - S^{1/2}(I - (P')^\top P')S^{1/2})\tilde{R}_p^{-1/2}\|_2 \leq \lambda_{\max}(I - \epsilon\tilde{R}_p^{-1})I = I - \epsilon\lambda_{\min}(\tilde{R}_p^{-1})I. \end{aligned}$$

Thus, we conclude that

$$\|P'(P')^\top\|_2 \leq \left(1 - \epsilon\lambda_{\min}(\tilde{R}_p^{-1})\right)\left(1 - \epsilon\lambda_{\min}(\tilde{R}_p^{-1})\right).$$

Next, one can see that

$$\lambda_{\min}(\epsilon\tilde{R}_p^{-1}) \leq \frac{\epsilon + 2\|Q\|_2 + 2\|S\|_2}{\epsilon}.$$

Thus, we get

$$\|P'\|_2^2 = \|P'(P')^\top\|_2 \leq \left(1 - \frac{\epsilon}{\epsilon + 2\|Q\|_2 + 2\|S\|_2}\right)^2.$$

The result follows. \square

Lemma B.5. *Let $\Sigma_0, \Sigma_1 \succ 0$. Then $P \mapsto \Xi(P, \Sigma_0, \Sigma_1) = \Sigma_1^{-1/2}P(I - P^\top P)^{-1}\Sigma_0^{-1/2}$ is bi-Lipschitz on the set $\{P \in \mathbb{R}^{D \times D} : \|P\|_2 \leq \sqrt{1 - \alpha}\}$, $0 < \alpha < 1$. Specifically,*

$$L\|P - P'\|_2 \leq \|A(P) - A(P')\|_2 \leq M_\alpha\|P - P'\|_2,$$

where

$$L = \frac{1}{\sqrt{2D}\|\Sigma_1\|_2^{1/2} \cdot \|\Sigma_0\|_2^{1/2}}, \quad M_\alpha = \|\Sigma_1^{-1}\|_2^{1/2} \cdot \|\Sigma_0^{-1}\|_2^{1/2} \left(\frac{1}{\alpha} + \frac{2}{\alpha^2}\right).$$

Before proving the lemma, we introduce some notations. Let h be a scalar function. For any $d \times d$ diagonal matrix $\Lambda = \text{diag}(\lambda_1, \dots, \lambda_d)$, we define

$$h(\Lambda) = \text{diag}(h(\lambda_1), \dots, h(\lambda_d)).$$

Respectively, given a $d \times d$ real symmetric matrix A with spectral decomposition $A = Q\Lambda Q^\top$, we set

$$h(A) = Qh(\Lambda)Q^\top.$$

Proof. Let $A = \Xi(P, \Sigma_0, \Sigma_1)$. To estimate M_α , we note that

$$dA = \Sigma_1^{-1/2} dP (I - P^\top P)^{-1} \Sigma_0^{-1/2} - \Sigma_1^{-1/2} P (I - P^\top P)^{-1} (dP^\top P + P^\top dP) (I - P^\top P)^{-1} \Sigma_0^{-1/2}.$$

By the conditions of the lemma, $0 \prec P^\top P \prec (1 - \alpha)I$, hence $\|(I - P^\top P)^{-1}\|_2 \leq \frac{1}{\alpha}$ and $\|P\|_2 \leq 1$. Thus,

$$\|dA\|_2 \leq \|\Sigma_1^{-1/2}\|_2 \|\Sigma_0^{-1/2}\|_2 \left(\frac{1}{\alpha} + \frac{2}{\alpha^2} \right) \|dP\|_2.$$

Since the ball $\{P : \|P\|_2 \leq \sqrt{1 - \alpha}\}$ is convex, this yields the bound M_α on the Lipschitz constant of $\Xi(\cdot, \Sigma_0, \Sigma_1)$.

To estimate L , we define $B = \Sigma_1^{1/2} A \Sigma_0^{1/2} = P (I - P^\top P)^{-1}$ and note that

$$B^\top B = (I - P^\top P)^{-1} P^\top P (I - P^\top P)^{-1} = (I - P^\top P)^{-2} - (I - P^\top P)^{-1}.$$

Next, define $h(x) = \frac{2}{1 + \sqrt{1 + 4x}}$, $x \geq 0$, so that $h^{-1}(y) = y^{-2} - y^{-1}$, $0 < y \leq 1$. Therefore,

$$\begin{aligned} I - P^\top P &= h(B^\top B), \\ P &= B (I - P^\top P) = Bh(B^\top B). \end{aligned} \tag{46}$$

For now, consider B such that its singular values are positive and distinct (note that the set of such matrices is dense in $\mathbb{R}^{D \times D}$). Then the SVD map $B \mapsto (U, \Lambda, V)$ such that $B = U\Lambda V^*$ is differentiable at B (see Magnus & Neudecker, 2019, Section 3.8.8), thus so is the polar decomposition map $B \mapsto (Q, S)$ such that $B = QS$, $Q \in O(D)$, $S \in \text{Sym}(D)$. As

$$P = Bh(B^\top B) = QSh(S^2) = U\Lambda h(\Lambda^2)V^*$$

and $xh(x^2)$ is differentiable, we obtain that

$$dP = dQSh(S^2) + Qd(Sh(S^2)).$$

Furthermore, $0 < h(x) \leq 1$ and $(xh(x^2))' = \frac{2}{(1 + \sqrt{1 + 4x^2})\sqrt{1 + 4x^2}} \in (0, 1]$, hence $0 \prec h(S^2) \prec I$ and $Sh(S^2)$ is 1-Lipschitz w.r.t. the Frobenius norm (Wihler, 2009, Thm. 1.1). Note that $\text{Tr}(QdS)^\top dQS = \text{Tr}(SdS)(Q^\top dQ) = 0$ since $Q^\top dQ$ is skew-symmetric, thus

$$\|dB\|_F^2 = \|dQS + QdS\|_F^2 = \|dQS\|_F^2 + \|QdS\|_F^2 = \|dQS\|_F^2 + \|dS\|_F^2.$$

Therefore,

$$\|dP\|_F = \|dQSh(S^2) + Qd(Sh(S^2))\|_F \leq \|dQS\|_F \|h(S^2)\|_2 + \|d(Sh(S^2))\|_F \leq \|dQS\|_F + \|dS\|_F \leq \sqrt{2} \|dB\|_F.$$

In particular,

$$\|dP\|_2 \leq \|dP\|_F \leq \sqrt{2} \|dB\|_F \leq \sqrt{2D} \|dB\|_2 \leq \sqrt{2D} \|\Sigma_1^{1/2}\|_2 \|\Sigma_0^{1/2}\|_2 \|dA\|_2.$$

By continuity of the SVD and thus of the map $Bh(B^\top B)$, this yields that

$$L^{-1} = \sqrt{2D} \|\Sigma_1^{1/2}\|_2 \|\Sigma_0^{1/2}\|_2. \quad \square$$

Corollary B.6. Fix $\Sigma_0, \Sigma_1 \succ 0$. Set $g(A) := \Xi(f(\Xi^{-1}(A; \Sigma_0, \Sigma_1)))$, where $\Xi^{-1}(\cdot; \Sigma_0, \Sigma_1)$ denotes the inverse map w.r.t. the first argument. Then g is Lipschitz continuous with constant $\frac{M_\alpha}{L} \gamma(\epsilon, \|\Sigma_0\|_2, \|\Sigma_1\|_2)$ on $\{A \mid \|\Xi^{-1}(A)\|_2 \leq \sqrt{1 - \alpha}\}$.

Corollary B.7. Let the starting point be

$$\begin{pmatrix} \Sigma_0 & P \\ P^\top & S \end{pmatrix} \succ 0.$$

Then after IMF step, we get

$$\|A(P'_n) - A(P_n^*)\|_2 \leq \frac{M_\alpha}{L} \gamma(\epsilon, \|\Sigma_0\|_2, \|S\|_2) \|A(P_n) - A(P_n^*)\|_2,$$

where

$$\alpha = \min \left\{ 1 - \|P_n\|_2^2, \frac{\epsilon}{\epsilon + 2\|\Sigma_0\|_2 + 2\|S\|_2} \right\}.$$

Corollary B.8 (Bound for $\|P_n\|_2^2$). *Let $q(x_0, x_1) = \mathcal{N}\left(\begin{pmatrix} \mu \\ \tilde{\mu} \end{pmatrix}, \begin{pmatrix} \Sigma & P \\ P^\top & \tilde{\Sigma} \end{pmatrix}\right)$ be a Gaussian distribution, $A = \Xi(P, \Sigma, \tilde{\Sigma})$ be its optimality matrix and $P_n = \Sigma^{-\frac{1}{2}} P \tilde{\Sigma}^{-\frac{1}{2}}$ be its normalized covariance matrix. Then the following bound holds true:*

$$\|P_n\|_2^2 \leq 1 - \frac{2}{1 + \sqrt{1 + 4\|\Sigma\|_2\|\tilde{\Sigma}\|_2\|A\|_2^2}}. \quad (47)$$

Proof. We recall the explicit formula (46) connecting P_n and A :

$$I - P_n^\top P_n = h(B^\top B), \quad (48)$$

where matrix $B := \tilde{\Sigma}A\Sigma$ and scalar function $h(x) := \frac{2}{1 + \sqrt{1 + 4x}}$, $x \geq 0$. Given a $D \times D$ positive definite matrix C with spectral decomposition $C = U\Lambda U^*$, we set $h(C) = Uh(\Lambda)U^*$. We start with estimate

$$\lambda_{\min}(h(B^\top B)) = \lambda_{\min}(I - P_n^\top P_n) = 1 - \lambda_{\max}(P_n^\top P_n) = 1 - \|P_n\|_2^2. \quad (49)$$

Since function h is monotonously decreasing on $[0, +\infty)$ and matrix $B^\top B$ has non-negative eigenvalues, we have $\lambda_{\min}(h(B^\top B)) = h(\lambda_{\max}(B^\top B))$ and continue with:

$$\lambda_{\min}(h(B^\top B)) = h(\lambda_{\max}(B^\top B)) = h(\|B^\top B\|_2) \geq h(\|A\|_2^2\|\Sigma\|_2\|\tilde{\Sigma}\|_2) = \frac{2}{1 + \sqrt{1 + 4\|\Sigma\|_2\|\tilde{\Sigma}\|_2\|A\|_2^2}}.$$

Combining bounds together, we conclude:

$$\|P_n\|_2^2 \leq 1 - \frac{2}{1 + \sqrt{1 + 4\|\Sigma\|_2\|\tilde{\Sigma}\|_2\|A\|_2^2}}.$$

□

B.4. IMF step analysis in 1D

Preliminaries. In case $D = 1$, we work with scalars $\mu_0, \mu_1, \sigma_0^2, \sigma_1^2$ instead of matrices $\mu_0, \mu_1, \Sigma_0, \Sigma_1$. The correlation matrix P can be restated as $P = \rho\sigma_0\sigma_1$, where $\rho \in (-1, 1)$ is the correlation coefficient. Using these notations, formula (10) for optimality coefficient $\chi \in \mathbb{R}$ (instead of matrix A) can be expressed as

$$\Xi(\rho, \sigma, \sigma') \stackrel{\text{def}}{=} \frac{\rho}{\sigma\sigma'(1 - \rho^2)} = \chi \in (-\infty, +\infty). \quad (50)$$

The function Ξ is monotonously increasing w.r.t. $\rho \in (-1, 1)$ and, thus, invertible, i.e., there exists a function $\Xi^{-1} : (-\infty, +\infty) \times \mathbb{R}_+ \times \mathbb{R}_+ \rightarrow (-1, 1)$ such that

$$\Xi^{-1}(\chi, \sigma, \sigma') = \frac{\sqrt{\chi^2\sigma^2(\sigma')^2 + 1/4} - 1/2}{\chi\sigma\sigma'}. \quad (51)$$

The inverse function is calculated via solving quadratic equation w.r.t. ρ .

In our paper, we consider both discrete and continuous IMF. By construction, IMF step does change marginals of the process it works with. However, for both continuous and discrete IMF, the new correlation converges to the correlation of the ϵ_* -EOT between marginals.

Lemma B.9 (Correlation improvement after (D)IMF step). *Consider a 2-dimensional Gaussian distribution with marginals $p = \mathcal{N}(\mu, \sigma^2)$ and $p' = \mathcal{N}(\mu', (\sigma')^2)$ and correlation $\rho \in (-1, 1)$ between its components. After continuous IMF or DIMF with single time point t , we obtain correlation ρ_{new} . The distance between ρ_{new} and EOT correlation $\rho_* = \Xi^{-1}(1/\epsilon_*, \sigma, \sigma')$ decreases as:*

$$|\rho_{new} - \rho_*| \leq \gamma \cdot |\rho - \rho_*|,$$

where factor γ for continuous and discrete IMF (with $N = 1$) is, respectively,

$$\gamma_c(\sigma, \sigma') = \frac{\sqrt{\sigma^2(\sigma')^2 + \epsilon_*^2/4} - \epsilon_*/2}{\sigma\sigma'}, \quad (52)$$

$$\gamma_d(\sigma, \sigma', t) = \frac{1}{1 + \frac{t^2(1-t)^2\sigma^2(\sigma')^2 + t(1-t)(t^2(\sigma')^2 + (1-t)^2\sigma^2)\epsilon + t^2(1-t)^2\epsilon_*^2}{(1-t)^2((1-t)\sigma^2 + t\sigma\sigma')^2 + t^2(t(\sigma')^2 + (1-t)\sigma\sigma')^2 + t(1-t)((1-t)\sigma + t\sigma')^2\epsilon_*}}. \quad (53)$$

Proof. Continuous case. Following (Peluchetti, 2023a, Eq. 42), we have the formula for ρ_{new} :

$$\rho_{new}(\rho) = \exp \left\{ -\epsilon_* \frac{\tanh^{-1}\left(\frac{c_1}{c_3}\right) + \tanh^{-1}\left(\frac{c_2}{c_3}\right)}{c_3} \right\} > 0, \quad (54)$$

$$\begin{aligned} c_1 &= \epsilon_* + 2(\sigma')^2(\rho\sigma^2 - (\sigma')^2), \quad c_3 = \sqrt{(\epsilon_* + 2(\rho + 1)\sigma^2(\sigma')^2)(\epsilon_* + 2(\rho - 1)\sigma^2(\sigma')^2)}, \\ c_2 &= \epsilon_* + 2\sigma^2(\rho(\sigma')^2 - \sigma^2). \end{aligned}$$

The map $\rho_{new}(\rho)$ is contraction over $\rho \in [-1, 1]$ with the contraction coefficient $\gamma_c(\sigma, \sigma') \stackrel{\text{def}}{=} \frac{\sqrt{\sigma^2(\sigma')^2 + \epsilon_*^2/4} - \epsilon_*/2}{\sigma\sigma'} < 1$. The unique fixed point of such map is $\rho_* = P^{(1/\epsilon_*, \sigma_0, \sigma_1)}$, since IMF does not change ϵ_* -EOT solution. Hence, we derive a bound

$$|\rho_{new}(\rho) - \rho_*| = |\rho_{new}(\rho) - \rho_{new}(\rho_*)| \leq \gamma_c(\sigma, \sigma') |\rho - \rho_*|.$$

Discrete case ($N = 1$). In this case, we use notations from (Gushchin et al., 2024), namely, we denote covariance matrix $\begin{pmatrix} \Sigma_0 & P \\ P & \Sigma_1 \end{pmatrix} \stackrel{\text{def}}{=} \begin{pmatrix} \sigma^2 & \rho\sigma\sigma' \\ \rho\sigma\sigma' & (\sigma')^2 \end{pmatrix}$.

The general formulas of DIMF step are given for time points $0 = t_0 < t_1 < \dots < t_N < t_{N+1} = 1$. Following (Gushchin et al., 2024), we have an explicit formula for reciprocal step. For any $1 \leq k \leq N$, we have joint covariance between time moments

$$\begin{aligned} \Sigma_{t_k, t_k} &= (1 - t_k)^2 \Sigma_0 + 2t_k(1 - t_k)P + t_k^2 \Sigma_1 + t_k(1 - t_k)\epsilon_*, \\ \Sigma_{t_{k+1}, t_k} &= (1 - t_k)(1 - t_{k+1})\Sigma_0 + [(1 - t_k)t_{k+1} + (1 - t_{k+1})t_k]P + t_k t_{k+1} \Sigma_1 + t_k(1 - t_{k+1})\epsilon_*, \\ \Sigma_{t_1, 0} &= (1 - t_1)\Sigma_0 + t_1 P, \\ \Sigma_{1, t_N} &= t_N \Sigma_1 + (1 - t_N)P. \end{aligned}$$

Matrices Σ_{t_{k+1}, t_k} and Σ_{t_k, t_k} depend on P . For Markovian step, we write down an analytical formula for the new covariance Σ_{new} between marginals:

$$f(P) \stackrel{\text{def}}{=} P_{new}(P) = \prod_{k=0}^N (\Sigma_{t_{k+1}, t_k} \cdot \Sigma_{t_k, t_k}^{-1}) \cdot \Sigma_0,$$

The derivative of $f'(P)$ is as follows:

$$\begin{aligned} f'(P) &= \left[\frac{(1 - t_N)}{\Sigma_{1, t_N}} - \frac{2t_N(1 - t_N)}{\Sigma_{t_N, t_N}} + \frac{t_1}{\Sigma_{t_1, 0}} \right] \cdot f(P) \\ &+ \sum_{k=1}^{N-1} \left[\frac{[(1 - t_k)t_{k+1} + t_k(1 - t_{k+1})]}{\Sigma_{t_{k+1}, t_k}} - \frac{2t_k(1 - t_k)P}{\Sigma_{t_k, t_k}} \right] \cdot f(P) \\ &= \sum_{k=0}^N \left[-\frac{t_{k+1}(1 - t_{k+1})}{\Sigma_{t_{k+1}, t_{k+1}}} + \frac{t_{k+1}(1 - t_k) + t_k(1 - t_{k+1})}{\Sigma_{t_{k+1}, t_k}} - \frac{t_k(1 - t_k)}{\Sigma_{t_k, t_k}} \right] \cdot f(P). \quad (55) \end{aligned}$$

In the case of single point $t = t_1$ ($N = 1$), we prove that the function $f(P)$ is a contraction map. The sufficient condition for the map to be contraction is to have derivative's norm bounded by $\gamma_d < 1$.

Firstly, we can write down the simplified formula $\rho_{new}(\rho)$ in our original notations:

$$\rho_{new}(\rho) = \frac{((1-t)\sigma + t\rho\sigma')(t\sigma' + (1-t)\rho\sigma)}{(1-t)\sigma^2 + 2t(1-t)\rho\sigma\sigma' + t^2(\sigma')^2 + t(1-t)\epsilon_*}. \quad (56)$$

Next, we simplify derivative (55):

$$\begin{aligned} \Sigma_{0,t} &= (1-t) \cdot \Sigma_0 + t \cdot P, \\ \Sigma_{t,1} &= t \cdot \Sigma_1 + (1-t) \cdot P, \\ \Sigma_{t,t} &= (1-t)^2 \cdot \Sigma_0 + 2(1-t)t \cdot P + t^2 \cdot \Sigma_1 + t(1-t)\epsilon_0 = (1-t) \cdot \Sigma_{0,t} + t \cdot \Sigma_{t,1} + t(1-t)\epsilon, \\ f'(P) &= \frac{(1-t)\Sigma_{0,t}}{\Sigma_{t,t}} + \frac{t\Sigma_{t,1}}{\Sigma_{t,t}} - 2 \cdot \frac{t\Sigma_{t,1} \cdot (1-t)\Sigma_{0,t}}{\Sigma_{t,t} \cdot \Sigma_{t,t}}. \end{aligned}$$

We define new variables $\tilde{\Sigma}_{0,t} \stackrel{\text{def}}{=} (1-t)\Sigma_{0,t}$, $\tilde{\Sigma}_{t,1} \stackrel{\text{def}}{=} t\Sigma_{t,1}$ and $\tilde{\epsilon}_* = t(1-t)\epsilon_*$. We note that while $P \in [-\sqrt{\Sigma_0\Sigma_1}, \sqrt{\Sigma_0\Sigma_1}]$ the value $\tilde{\Sigma}_{0,t} + \tilde{\Sigma}_{t,1} = (1-t)^2 \cdot \Sigma_0 + 2(1-t)t \cdot P + t^2 \cdot \Sigma_1 \geq 0$. Then, we restate f' as:

$$f' = \frac{\tilde{\Sigma}_{0,t}}{\tilde{\Sigma}_{0,t} + \tilde{\Sigma}_{t,1} + \tilde{\epsilon}_*} + \frac{\tilde{\Sigma}_{t,1}}{\tilde{\Sigma}_{0,t} + \tilde{\Sigma}_{t,1} + \tilde{\epsilon}_*} - \frac{2\tilde{\Sigma}_{0,t}\tilde{\Sigma}_{t,1}}{(\tilde{\Sigma}_{0,t} + \tilde{\Sigma}_{t,1} + \tilde{\epsilon}_*)^2} \quad (57)$$

$$= \frac{(\tilde{\Sigma}_{0,t} + \tilde{\Sigma}_{t,1})(\tilde{\Sigma}_{0,t} + \tilde{\Sigma}_{t,1} + \tilde{\epsilon}_*) - 2\tilde{\Sigma}_{0,t}\tilde{\Sigma}_{t,1}}{(\tilde{\Sigma}_{0,t} + \tilde{\Sigma}_{t,1} + \tilde{\epsilon}_*)^2}$$

$$= \frac{\tilde{\Sigma}_{0,t}^2 + \tilde{\Sigma}_{t,1}^2 + (\tilde{\Sigma}_{0,t} + \tilde{\Sigma}_{t,1})\tilde{\epsilon}_*}{(\tilde{\Sigma}_{0,t} + \tilde{\Sigma}_{t,1} + \tilde{\epsilon}_*)^2} \quad (58)$$

$$= \frac{\tilde{\Sigma}_{0,t}^2 + \tilde{\Sigma}_{t,1}^2 + (\tilde{\Sigma}_{0,t} + \tilde{\Sigma}_{t,1})\tilde{\epsilon}_*}{\tilde{\Sigma}_{0,t}^2 + 2\tilde{\Sigma}_{0,t}\tilde{\Sigma}_{t,1} + \tilde{\Sigma}_{t,1}^2 + 2(\tilde{\Sigma}_{0,t} + \tilde{\Sigma}_{t,1})\tilde{\epsilon}_* + \tilde{\epsilon}_*^2} \quad (59)$$

$$= \frac{1}{1 + \frac{2\tilde{\Sigma}_{0,t}\tilde{\Sigma}_{t,1} + (\tilde{\Sigma}_{0,t} + \tilde{\Sigma}_{t,1})\tilde{\epsilon}_* + \tilde{\epsilon}_*^2}{\tilde{\Sigma}_{0,t}^2 + \tilde{\Sigma}_{t,1}^2 + (\tilde{\Sigma}_{0,t} + \tilde{\Sigma}_{t,1})\tilde{\epsilon}_*}}. \quad (60)$$

We note that all terms in (58) are greater than 0:

$$0 < f'(P), \quad P \in [-\sqrt{\Sigma_0\Sigma_1}, \sqrt{\Sigma_0\Sigma_1}]. \quad (61)$$

In negative segment $P \in [-\sqrt{\Sigma_0\Sigma_1}, 0]$, the derivative f' is greater than in positive segment $[0, \sqrt{\Sigma_0\Sigma_1}]$, and edge value $f(-\sqrt{\Sigma_0\Sigma_1}) > -\sqrt{\Sigma_0\Sigma_1}$. Thus, in negative segment, the convergence to the fixed point $\rho_*\sqrt{\Sigma_0\Sigma_1} > 0$ is faster, than in positive segment.

For $P \in [0, \sqrt{\Sigma_0\Sigma_1}]$, we can bound the fraction in denominator of (60) by taking its numerator's minimum at $P = 0$ and its denominator's maximum at $P = \sqrt{\Sigma_0\Sigma_1}$, i.e.,

$$\begin{aligned} 0 < f' &\leq \gamma_d(\Sigma_0, \Sigma_1, t) < 1, \\ \gamma_d(\Sigma_0, \Sigma_1, t) &= \frac{1}{1 + \frac{t^2(1-t)^2\Sigma_0\Sigma_1 + t(1-t)(t^2\Sigma_1 + (1-t)^2\Sigma_0)\epsilon + t^2(1-t)^2\epsilon_*^2}{(1-t)^2((1-t)\Sigma_0 + t\sqrt{\Sigma_0\Sigma_1})^2 + t^2(t\Sigma_1 + (1-t)\sqrt{\Sigma_0\Sigma_1})^2 + t(1-t)((1-t)\sqrt{\Sigma_0} + t\sqrt{\Sigma_1})^2\epsilon_*}}. \end{aligned}$$

We note that $\gamma_d(\Sigma_0, \Sigma_1, t)$ is increasing function w.r.t. Σ_0, Σ_1 .

If we put into the function f argument $P_* = \rho_*\sqrt{\Sigma_0\Sigma_1}$ corresponding to the ϵ_* -EOT correlation, DIMF does not change it. Hence, P_* is the fixed point of $f(P)$, and we have

$$|P_{new} - P_*| = |f(P) - f(P_*)| \leq \gamma_d(\Sigma_0, \Sigma_1, t)|\Sigma - \Sigma_*|.$$

Dividing both sides by $\sqrt{\Sigma_0\Sigma_1}$, we get

$$|\rho_{new} - \rho_*| \leq \gamma_d(\Sigma_0, \Sigma_1, t)|\rho - \rho_*|.$$

□

Lemma B.10 (χ improvement after (D)IMF step). *Consider a 2-dimensional Gaussian distribution with marginals $p = \mathcal{N}(\mu, \sigma^2)$ and $p' = \mathcal{N}(\mu', (\sigma')^2)$ and correlation $\rho \in (-1, 1)$ between its components. After continuous IMF or DIMF with a single time point t , we obtain new correlation ρ_{new} , such that $|\rho_{new} - \rho_*| \leq \gamma|\rho - \rho_*|$ where $\rho_* = P(1/\epsilon_*, \sigma, \sigma')$ and $\gamma < 1$ is from (52) for IMF and from (53) for DIMF. We have bound in terms of $\chi = \Xi(\rho, \sigma, \sigma')$ and $\chi_{new} = \Xi(\rho_{new}, \sigma, \sigma')$:*

$$\begin{aligned} |\chi_{new} - 1/\epsilon_*| &\leq l(\rho, \rho_*, \gamma) \cdot |\chi - 1/\epsilon_*|, \\ l(\rho, \rho_*, \gamma) &= \left[1 - (1 - \gamma) \frac{(1 - \max\{\rho_*, |\rho|\})^2}{1 + \max\{\rho_*, |\rho|\}^2} \right] < 1. \end{aligned} \quad (62)$$

Proof. Monotone. The function ρ_{new} from (54) for continuous IMF and from (56) for DIMF is monotonously increasing on $(-1, 1)$. For continuous IMF, with the growth of ρ , c_3 grows faster than c_1 or c_2 , hence, $\frac{c_1}{c_3}, \frac{c_2}{c_3}$ and $\tanh^{-1}\left(\frac{c_1}{c_3}\right), \tanh^{-1}\left(\frac{c_2}{c_3}\right)$ decrease. Thus, the power in the exponent of ρ_{new} and ρ_{new} itself increase. For DIMF, the derivative of ρ_{new} greater than zero based on (61).

The monotone means that the value ρ_{new} always remains from the same side from ρ :

$$\begin{cases} \rho > \rho_* &\implies \rho_{new}(\rho) > \rho_* = \rho_{new}(\rho_*), \\ \rho \leq \rho_* &\implies \rho_{new}(\rho) \leq \rho_*, \end{cases} \quad (63)$$

The same inequalities hold true for $\chi = \Xi(\rho, \sigma, \sigma')$, $\chi_{new} = \Xi(\rho_{new}, \sigma, \sigma')$ and $\chi_* = 1/\epsilon_*$ as well: if $\chi < \chi_*$, then $\chi_{new} < \chi_*$ and vice versa, since $\Xi(\rho, \sigma, \sigma')$ is monotonously increasing w.r.t. ρ .

Ξ Properties. In this proof, we omit arguments σ, σ' of $\Xi^{-1}(\chi, \sigma, \sigma')$ and $\Xi(\rho, \sigma, \sigma')$, because they do not change during IMF step. The second derivative of the function $\Xi(\rho)$ is

$$\frac{d^2\Xi}{d\rho^2}(\rho) = \frac{2\rho(3 + \rho^2)}{\sigma\sigma'(1 - \rho^2)^3}.$$

Hence, we have $\frac{d^2\Xi}{d\rho^2}(\rho) \leq 0$ for $\rho \in (-1, 0]$ and $\frac{d^2\Xi}{d\rho^2}(\rho) \geq 0$ for $\rho \in [0, 1)$. It means that the function $\Xi(\rho)$ is concave on $(-1, 0]$ and convex on $[0, 1)$.

The function $\Xi(\rho)$ is monotonously increasing w.r.t. ρ , thus, decreasing of the radius $h \stackrel{\text{def}}{=} |\rho - \rho_*|$ around ρ_* causes the decreasing of $|\chi - \chi_*|$ around χ_* . We consider two cases: $\chi > \chi_*$ and $\chi < \chi_*$.

Case $\chi > \chi_*$. We have $\rho = \rho_* + h, \chi = \Xi(\rho_* + h) = \Xi(\rho)$ and $\Xi(\rho_* + \gamma h) \geq \chi_{new}$. We compare the difference using convexity on $[0, 1)$:

$$\begin{aligned} \chi - \chi_{new} &\geq \Xi(\rho_* + h) - \Xi(\rho_* + \gamma h) \geq (\rho_* + h - (\rho_* + \gamma h)) \cdot \frac{d\Xi}{d\rho}(\rho_* + \gamma h) \\ &= (1 - \gamma)h \cdot \frac{d\Xi}{d\rho}(\rho_* + \gamma h). \end{aligned}$$

Since the derivative of Ξ is always positive, we continue the bound:

$$\Xi(\rho_* + h) - \Xi(\rho_* + \gamma h) \geq \min_{\rho' \in [\rho_*, \rho_* + h]} \left| \frac{d\Xi}{d\rho}(\rho') \right| (1 - \gamma)|\rho - \rho_*|.$$

Next, we use Lipschitz property of Ξ , i.e.,

$$|\chi - \chi_*| = |\Xi(\rho) - \Xi(\rho_*)| \leq \max_{\rho' \in [\rho_*, \rho_* + h]} \left| \frac{d\Xi}{d\rho}(\rho') \right| |\rho - \rho_*|,$$

and combine it with the previous bound

$$\chi - \chi_{new} \geq \Xi(\rho_* + h) - \Xi(\rho_* + \gamma h) \geq \frac{\min_{\rho' \in [\rho_*, \rho]} \left| \frac{d\Xi}{d\rho}(\rho') \right|}{\max_{\rho' \in [\rho_*, \rho]} \left| \frac{d\Xi}{d\rho}(\rho') \right|} (1 - \gamma)|\chi - \chi_*|.$$

Case $\chi < \chi_*$. We have $\rho = \rho_* - h, \chi = \Xi(\rho_* - h) = \Xi(\rho)$ and $\Xi(\rho_* - \gamma h) \leq \chi_{new}$. There are three subcases for χ, χ_{new} positions around 0:

1. For positions $\chi_* > \chi_{new} > \chi \geq 0$, we use *convexity* of Ξ on $[0, 1]$ and obtain

$$\begin{aligned} \chi_{new} - \chi &\geq \Xi(\rho_* - \gamma h) - \Xi(\rho_* - h) \geq (1 - \gamma)h \cdot \frac{d\Xi}{d\rho}(\rho_* - h) \\ &\geq \min_{\rho' \in [\rho_* - h, \rho_*]} \left| \frac{d\Xi}{d\rho}(\rho') \right| (1 - \gamma)|\rho - \rho_*|. \end{aligned}$$

2. For positions $\chi_* > 0 \geq \chi_{new} > \chi$, we use *concavity* of Ξ on $(-1, 0]$ and obtain

$$\begin{aligned} \chi_{new} - \chi &\geq \Xi(\rho_* - \gamma h) - \Xi(\rho_* - h) \geq (1 - \gamma)h \cdot \frac{d\Xi}{d\rho}(\rho_* - \gamma h) \\ &\geq \min_{\rho' \in [\rho_* - h, \rho_*]} \left| \frac{d\Xi}{d\rho}(\rho') \right| (1 - \gamma)|\rho - \rho_*|. \end{aligned}$$

3. For positions $\chi_* > \chi_{new} > 0 > \chi$, we use *concavity* of Ξ on $(-1, 0]$ and *convexity* of Ξ on $[0, 1]$ and obtain

$$\begin{aligned} \chi_{new} - \chi &\geq \Xi(\rho_* - \gamma h) - \Xi(\rho_* - h) = [\Xi(\rho_* - \gamma h) - \Xi(0)] + [\Xi(0) - \Xi(\rho_* - h)] \\ &\geq (\rho_* - \gamma h) \cdot \frac{d\Xi}{d\rho}(0) + (h - \rho_*) \cdot \frac{d\Xi}{d\rho}(0) = (1 - \gamma)h \cdot \frac{d\Xi}{d\rho}(0) \\ &\geq \min_{\rho' \in [\rho_* - h, \rho_*]} \left| \frac{d\Xi}{d\rho}(\rho') \right| (1 - \gamma)|\rho - \rho_*|. \end{aligned}$$

Overall, we make the bound

$$\begin{aligned} \chi_{new} - \chi &\geq \min_{\rho' \in [\rho_* - h, \rho_*]} \left| \frac{d\Xi}{d\rho}(\rho') \right| (1 - \gamma)|\rho - \rho_*| \\ &\geq \frac{\min_{\rho' \in [\rho, \rho_*]} \left| \frac{d\Xi}{d\rho}(\rho') \right|}{\max_{\rho' \in [\rho, \rho_*]} \left| \frac{d\Xi}{d\rho}(\rho') \right|} (1 - \gamma)|\chi - \chi_*|. \end{aligned}$$

For the function $\Xi(\rho) = \frac{\rho}{\sigma_0 \sigma_1 (1 - \rho^2)}$, the centrally symmetrical derivative is

$$\frac{d\Xi}{d\rho}(\rho) = \frac{1 + \rho^2}{\sigma_0 \sigma_1 (1 - \rho^2)^2}.$$

The derivative $\frac{d\Xi}{d\rho}$ has its global minimum at $\rho = 0$. It grows as $\rho \rightarrow \pm 1$, hence, the maximum value is achieved at points which are farthest from 0:

$$\begin{aligned} \max_{\rho' \in [\rho_*, \rho]} \left| \frac{d\Xi}{d\rho}(\rho') \right| &\leq \frac{d\Xi}{d\rho}(\rho), \\ \max_{\rho' \in [\rho, \rho_*]} \left| \frac{d\Xi}{d\rho}(\rho') \right| &\leq \max \left\{ \frac{d\Xi}{d\rho}(\rho_*), \frac{d\Xi}{d\rho}(|\rho|) \right\}, \\ \min_{\rho' \in [-1, +1]} \left| \frac{d\Xi}{d\rho}(\rho') \right| &\geq \frac{1}{\sigma_0 \sigma_1}. \end{aligned}$$

Thus, we prove the bound

$$\begin{aligned} |\chi - \chi_*| - |\chi_{new} - \chi_*| &= |\chi_{new} - \chi| \geq \frac{(1 - \max\{\rho_*, |\rho|\}^2)^2}{1 + \max\{\rho_*, |\rho|\}^2} (1 - \gamma)|\chi - \chi_*|. \\ |\chi_{new} - \chi_*| &\leq \left[1 - (1 - \gamma) \frac{(1 - \max\{\rho_*, |\rho|\}^2)^2}{1 + \max\{\rho_*, |\rho|\}^2} \right] |\chi - \chi_*|. \end{aligned}$$

□

B.5. Proof of IPMF Convergence Theorem 3.2, $D > 1$

Proof. We denote by Q_0 marginal matrix at $t = 0$ after the first IPF step. Firstly, we note that all marginal matrices Q at $t = 0$ and S at $t = 1$ emerging during IPMF procedure are bounded by the initial ones (Lemma B.2):

$$\|S\|_2 \leq \frac{\|\Sigma_1\|_2}{\min\{\lambda_{\min}(S_0^{-\frac{1}{2}}\Sigma_1S_0^{-\frac{1}{2}}), 1\}} =: u_S, \quad \|S^{-1}\|_2 \leq \max\{\lambda_{\max}(S_0^{-\frac{1}{2}}\Sigma_1S_0^{-\frac{1}{2}}), 1\}\|\Sigma_1^{-1}\|_2 =: r_S, \quad (64)$$

$$\|Q\|_2 \leq \frac{\|\Sigma_0\|_2}{\min\{\lambda_{\min}(Q_0^{-\frac{1}{2}}\Sigma_0Q_0^{-\frac{1}{2}}), 1\}} =: u_Q, \quad \|Q^{-1}\|_2 \leq \max\{\lambda_{\max}(Q_0^{-\frac{1}{2}}\Sigma_0Q_0^{-\frac{1}{2}}), 1\}\|\Sigma_0^{-1}\|_2 =: r_Q. \quad (65)$$

Optimality convergence and condition on ϵ . Consider any IMF step during IPMF procedure which we denote by

$$\begin{pmatrix} Q & P \\ P^\top & S \end{pmatrix} \xrightarrow{IMF} \begin{pmatrix} Q & P' \\ (P')^\top & S \end{pmatrix}, \quad P_n := Q^{-\frac{1}{2}}PS^{-\frac{1}{2}}.$$

We want to find such ϵ , that, after this step, the optimality matrix $A' = \Xi(P', Q, S)$ becomes close to solution $A_* = \epsilon^{-1}I_D$ than starting $A = \Xi(P, Q, S)$. This transition from A to A' satisfies (Corollary B.7):

$$\|A' - A_*\|_2 \leq \left(\frac{6\sqrt{D} \cdot \kappa(Q^{\frac{1}{2}})\kappa(S^{\frac{1}{2}})}{\alpha^4} \right) \gamma(\epsilon, \|Q\|_2, \|S\|_2) \|A - A_*\|_2, \quad (66)$$

$$\gamma(\epsilon, \|Q\|_2, \|S\|_2) = \frac{(\|Q\|_2^{1/2} + \|S\|_2^{1/2})^2}{\epsilon} + \frac{2}{\epsilon^2} \|Q\|_2^{1/2} \|S\|_2^{1/2} (\|S\|_2^{1/2} + \|Q\|_2^{1/2})^2,$$

where $\kappa(\cdot)$ is condition number of matrix and $\alpha = \min\left\{1 - \|P_n\|_2^2, \frac{\epsilon}{\epsilon + 2(\|Q\|_2 + \|S\|_2)}\right\}$. The second term of α can be neglected if we take $\epsilon \geq u_Q + u_S \geq \|Q\|_2 + \|S\|_2$ and make it larger than $1/3$. To estimate $1 - \|P_n\|_2^2$ in the second term, we use lower bound (Corollary B.8):

$$\begin{aligned} \alpha &\geq \frac{2}{1 + \sqrt{1 + 4\|Q\|_2\|S\|_2\|A\|_2^2}} \geq \frac{1}{\sqrt{1 + 4\|Q\|_2\|S\|_2\|A\|_2^2}}, \\ \|A' - A_*\|_2 &\leq \underbrace{6\sqrt{D} \cdot \kappa(Q^{\frac{1}{2}})\kappa(S^{\frac{1}{2}})}_{:=l(Q,S,A,\epsilon)} \cdot (1 + 4\|Q\|_2\|S\|_2\|A\|_2^2)^2 \cdot \gamma(\|Q\|_2, \|S\|_2, \epsilon) \cdot \|A - A_*\|_2. \end{aligned} \quad (67)$$

Universal bounds (65) and (64) state that matrices Q and S lie on matrix compacts $B_Q := \{Q \succ 0 \mid \|Q\|_2 \leq u_Q, \|Q^{-1}\|_2 \leq r_Q\}$ and $B_S := \{S \succ 0 \mid \|S\|_2 \leq u_S, \|S^{-1}\|_2 \leq r_S\}$, respectively. Moreover, the function $l(Q, S, A, \epsilon)$ is continuous w.r.t. all its parameters on these compacts. Hence, we can get rid of Q, S dependency, since the following maximum is attained

$$l(A, \epsilon) = \max_{Q \in B_Q, S \in B_S} l(Q, S, A, \epsilon).$$

Now we deal with $\|A\|_2$ dependency. If at the first IMF step with initial optimality matrix A_0 coefficient $l(A_0, \epsilon)$ will be less than 1, then next matrix A' will be bounded by the norm

$$\|A'\|_2 \leq \|A' - A_*\|_2 + \|A_*\|_2 \leq \|A_0 - A_*\|_2 + \|A_*\|_2 \leq \|A_0\|_2 + 2\epsilon^{-1}.$$

Moreover, the coefficient $l(A, \epsilon)$ is increasing w.r.t. $\|A\|_2$, hence if we take maximal $\|A_0\|_2 + 2\epsilon^{-1}$ and bound l for it from the beginning, then all the following IMF steps will be contractive with this coefficient by induction (IPF steps do not change A , Lemma B.3).

The final condition (68) on ϵ is

$$\beta(Q_0, S_0, P_0, \epsilon) := \max_{Q \in B_Q, S \in B_S} \left[6\sqrt{D} \cdot \kappa(Q^{\frac{1}{2}})\kappa(S^{\frac{1}{2}}) \cdot (1 + 4\|Q\|_2\|S\|_2(\|A_0\|_2 + 2\epsilon^{-1})^2)^2 \cdot \gamma(\epsilon, \|Q\|_2, \|S\|_2) \right] < 1.$$

We can estimate above maximum and get lower bound for ϵ :

$$\beta(Q_0, S_0, P_0, \epsilon) \leq 6\sqrt{D} \cdot u_Q r_Q u_S r_S \cdot (1 + 4u_Q u_S (\|A_0\|_2 + 2\epsilon^{-1})^2)^2 \cdot 8 \frac{u_Q u_S}{\epsilon} \leq 1,$$

$$\epsilon = O\left(\sqrt{D \cdot r_Q r_S} \cdot u_Q^{\frac{5}{2}} u_S^{\frac{5}{2}} \|A_0\|_2^4\right), \epsilon \geq u_Q + u_S + \|A_0\|_2^{-1}. \quad (68)$$

If the above ϵ -condition (68) holds true, then A_k exponentially converges to A_* (square appears since IPMF step includes two IMF steps):

$$\|A_k - A_*\|_2 \leq \beta(Q_0, S_0, P_0, \epsilon)^{2k} \|A_0 - A_*\|_2.$$

Marginals convergence. Furthermore, we prove that marginals converge to ground truth Σ_1 as well. We note that, during any condition $\begin{pmatrix} Q & P \\ P^\top & S \end{pmatrix}$ of IPMF procedure, the norm of the normalized matrix $P_n = Q^{-\frac{1}{2}} P S^{-\frac{1}{2}}$ is bounded:

$$\|P_n\|_2^2 \leq 1 - \frac{2}{1 + \sqrt{1 + 4\|Q\|_2\|S\|_2\|A\|_2^2}}.$$

Since $\|Q\|_2 \leq u_Q$ (65), $\|S\|_2 \leq u_S$ (64) and $\|A\|_2 \leq \|A_0\|_2 + 2\epsilon^{-1}$ (due to contractivity of A), we can upper bound the normalized norm

$$\|P_n\|_2^2 \leq 1 - \frac{2}{1 + \sqrt{1 + 4u_Q u_S (\|A_0\|_2 + 2\epsilon^{-1})^2}} = \alpha(Q_0, S_0, P_0, \epsilon) < 1.$$

Finally, we apply bounds from IPF steps Lemma B.1 at k -th step and put maximal norm value $\alpha(Q_0, S_0, P_0, \epsilon)$:

$$\begin{aligned} \|S_k^{-\frac{1}{2}} \Sigma_1 S_k^{-\frac{1}{2}} - I_D\|_2 &\leq \alpha(Q_0, S_0, P_0, \epsilon)^2 \cdot \|S_0^{-\frac{1}{2}} \Sigma_1 S_0^{-\frac{1}{2}} - I_D\|_2, \\ \|\Sigma_1^{-\frac{1}{2}} (\nu_k - \mu_1)\|_2 &\leq \alpha(Q_0, S_0, P_0, \epsilon) \cdot \|\Sigma_1^{-\frac{1}{2}} (\nu_0 - \mu_1)\|_2. \end{aligned}$$

□

B.6. Proof of IPMF Convergence Theorem 3.2, $D = 1$

Proof. Notations. We denote the variance of the 0-th marginal after the k -th IPMF step as s'_k . For the first one, we have formula $s'_0 = \sqrt{\sigma_0^2 - \sigma_0^2 \tilde{\rho}_0^2 \left(1 - \frac{\sigma_1^2}{s^2}\right)}$, where $\tilde{\rho}_0$ is the correlation after the first IMF step. More explicitly, $\tilde{\rho}_0 \stackrel{\text{def}}{=} \rho_{new}(\rho_0)$, where ρ_{new} is taken from (54) for continuous IMF and from (56) for DIMF. We denote optimality coefficients $\chi_k \stackrel{\text{def}}{=} \Xi(\rho_k, \sigma_0, s_k)$ and $\chi_* \stackrel{\text{def}}{=} 1/\epsilon_*$.

Ranges. We note that IMF step keeps s, ν , while IPF keeps χ . Due to update equations for χ (63) and for s, ν (37), the parameters s_k, χ_k remain on the same side from $\sigma_1, \frac{1}{\epsilon_*}$, respectively. Namely, we have ranges for the variances $s_k \in [\sigma_1^{\min}, \sigma_1^{\max}] \stackrel{\text{def}}{=} [\min\{\sigma_1, s_0\}, \max\{\sigma_1, s_0\}]$, $s'_k \in [\sigma_0^{\min}, \sigma_0^{\max}] \stackrel{\text{def}}{=} [\min\{\sigma_0, s'_0\}, \max\{\sigma_0, s'_0\}]$ and parameters $\chi_k \in [\chi^{\min}, \chi^{\max}] \stackrel{\text{def}}{=} [\min\{\chi_*, |\chi_0|\}, \max\{\chi_*, |\chi_0|\}]$.

Update bounds. We use update bounds for χ (62) twice, for s (37) and for ν (40), however, we need to limit above the coefficients $|\Xi^{-1}(\chi, \sigma, \sigma')|$ and $l(\Xi^{-1}(\chi, \sigma, \sigma'), \Xi^{-1}(\chi_*, \sigma, \sigma'), \gamma(\sigma, \sigma'))$ over the considered ranges of the parameters $\sigma \in [\sigma_0^{\min}, \sigma_0^{\max}]$, $\sigma' \in [\sigma_1^{\min}, \sigma_1^{\max}]$ and $\chi \in [\chi^{\min}, \chi^{\max}]$. The functions Ξ^{-1}, l, γ are defined in (51), (62), (52) (or (53) with fixed t), respectively.

Since the function $|\Xi^{-1}(\chi, \sigma, \sigma')|$ is increasing w.r.t. σ, σ' and χ symmetrically around 0, we take maximal values $\sigma_0^{\max}, \sigma_1^{\max}$ and χ^{\max} . Similarly, the function $l(\Xi^{-1}(\chi, \sigma, \sigma'), \Xi^{-1}(\chi_*, \sigma, \sigma'), \gamma(\sigma, \sigma'))$ is increasing w.r.t. all arguments symmetrically around 0. Hence, we maximize the function $|\Xi^{-1}|$ and the function γ , which is also increasing w.r.t. σ and σ' .

Final bounds. The final bound after k step of IPMF are:

$$\begin{aligned} |s_k^2 - \sigma_1^2| &\leq \alpha^{2k} |s_0^2 - \sigma_1^2|, \\ |\nu_k - \mu_1| &\leq \alpha^k |\nu_0 - \mu_1|, \\ |\chi_k - 1/\epsilon_*| &\leq \beta^{2k} |\chi_0 - 1/\epsilon_*|, \end{aligned}$$

where $\beta \stackrel{\text{def}}{=} l(\Xi^{-1}(\chi^{\max}, \sigma_0^{\max}, \sigma_1^{\max}), \Xi^{-1}(\chi_*, \sigma_0^{\max}, \sigma_1^{\max}), \gamma(\sigma_0^{\max}, \sigma_1^{\max}))$ and $\alpha \stackrel{\text{def}}{=} \Xi^{-1}(\chi^{\max}, \sigma_0^{\max}, \sigma_1^{\max})$ taking l from (62), γ from (52) for continuous IMF and from (53) with fixed t for discrete IMF. □

C. Experimental supplementary

C.1. Illustrative $2D$ example visualization.

We provide the visualization of the starting processes and corresponding learned processes for *Gaussian* \rightarrow *Swiss roll* translation in Fig. 7. One can observe that all the particle trajectories are relatively straight and therefore close to the Schrödinger Bridge problem solution.

C.2. SB benchmark $B\mathbb{W}_2^2$ -UVP

We additionally study how well implementations of IPMF procedure starting from different starting processes map initial distribution p_0 into p_1 by measuring the metric $B\mathbb{W}_2^2$ -UVP also proposed by the authors of the benchmark (Gushchin et al., 2023b). We present the results in Table 2. One can observe that DSBM initialized from different starting processes has quite close results and so is the case for ASBM experiments with $\epsilon \in \{1, 10\}$, but with $\epsilon = 0.1$ one can notice that ASBM starting from IPF and *Ind* $p_0 \rightarrow p_0$ experience a decline in $B\mathbb{W}_2^2$ -UVP metric.

		$\epsilon = 0.1$				$\epsilon = 1$				$\epsilon = 10$				
Algorithm Type		$D=2$	$D=16$	$D=64$	$D=128$	$D=2$	$D=16$	$D=64$	$D=128$	$D=2$	$D=16$	$D=64$	$D=128$	
Best algorithm on benchmark [†]		Varies	0.016	0.05	0.25	0.22	0.005	0.09	0.56	0.12	0.01	0.02	0.15	0.23
DSBM-IMF			0.1	0.14	0.44	3.2	0.13	0.1	0.91	6.67	0.1	5.17	66.7	356
DSBM-IPF			0.35	0.6	0.6	1.62	0.01	0.18	0.91	6.64	0.2	3.78	81	206
DSBM- <i>Ind</i> $p_0 \rightarrow p_0$			0.08	0.38	0.62	1.72	0.13	0.18	0.84	7.45	0.04	3.72	99.3	251
SF ² M-Sink [†]		IPMF	0.04	0.18	0.39	1.1	0.07	0.3	4.5	17.7	0.17	4.7	316	812
ASBM-IMF [†]			0.016	0.1	0.85	11.05	0.02	0.34	1.57	3.8	0.013	0.25	1.7	4.7
ASBM-IPF			0.05	0.73	32.05	10.67	0.02	0.53	4.19	10.11	0.002	0.18	2.2	5.08
ASBM- <i>Ind</i> $p_0 \rightarrow p_0$			0.36	0.76	16.33	22.63	0.07	0.48	1.93	5.36	0.04	0.23	1.04	2.29

Table 2: Comparisons of $B\mathbb{W}_2^2$ -UVP \downarrow (%) between the ground truth static SB solution $p^T(x_0, x_1)$ and the learned solution on the SB benchmark. The best metric over is **bolded**. Results marked with [†] are taken from (Gushchin et al., 2024) or (Gushchin et al., 2023b).

C.3. Celeba SDEdit starting processes description

The IPMF framework does not require the starting process to have p_0, p_1 marginals or to be a Schrödinger bridge. One can then try other starting processes that would improve the practical performance of the IPMF algorithm. Properties of the starting process that would be desirable are (1) $q(x_0) = p_0(x_0)$ and marginal $q(x_1)$ to be close to $p_1(x_1)$ and (2) $q(x_0, x_1)$ to be close to SB. In the IMF or IPF, we had to choose one of these properties because we can not easily satisfy them both.

We propose to take a basic image-to-image translation method and use it as a coupling to induce a starting process for the IPMF procedure. Such a coupling could provide the two properties mentioned above. We use SDEdit (Meng et al., 2021) which requires an already trained diffusion model (SDE prior). Given an input image x , SDEdit first adds noise to the input and then denoises the resulting image by the SDE prior to make it closer to the target distribution of the SDE prior. Various models can be used as an SDE prior. We explore two options: trainable and train-free. As the first option, we train the DDPM (Ho et al., 2020) model on the Celeba 64×64 size female only part. As the second option we take an already trained Stable Diffusion (SD) V1.5 model (Rombach et al., 2022) with text prompts conditioned on which model generates 512×512 images similar to the CelebA female part. We then apply SDEdit with the Celeba male images as input to produce similar female images using trainable DDPM and train-free SDv1.5 approaches, we call the starting processes generated by these SDEdit induced couplings DDPM-SDEdit and SD-SDEdit. Hyperparameters of SDEdit, DDPM and SDv1.5 are provided in Appendix C.9.

The visualization of the DSBM and ASBM implementations of the IPMF procedure starting from DDPM-SDEdit and SD-SDEdit processes are in Figure 5. The quantitative evaluation of FID is given in Figure 6, the evaluation of CMMD – in Figure 8a and evaluation of MSE – in Figure 8b.

C.4. Celeba experiment additional quantitative study

In Figure 8, we provide additional quantitative study of IPMF convergence in CMMD (Jayasumana et al., 2024) and Mean Squared Error between inputs and outputs of translation by plotting them as a function of IPMF iteration. Both metrics are calculated on Celeba *male* \rightarrow *female* (64×64) test set. We notice CMMD plot resembles that of FID, see Figure 6. MSE plot can be divided into two groups: 1) IMF starting process, ASBM with *Ind* $p_0 \rightarrow p_0$ and 2) all the other experiments mostly including SDEdit starting processes with significantly lower distance between inputs and outputs of translation.

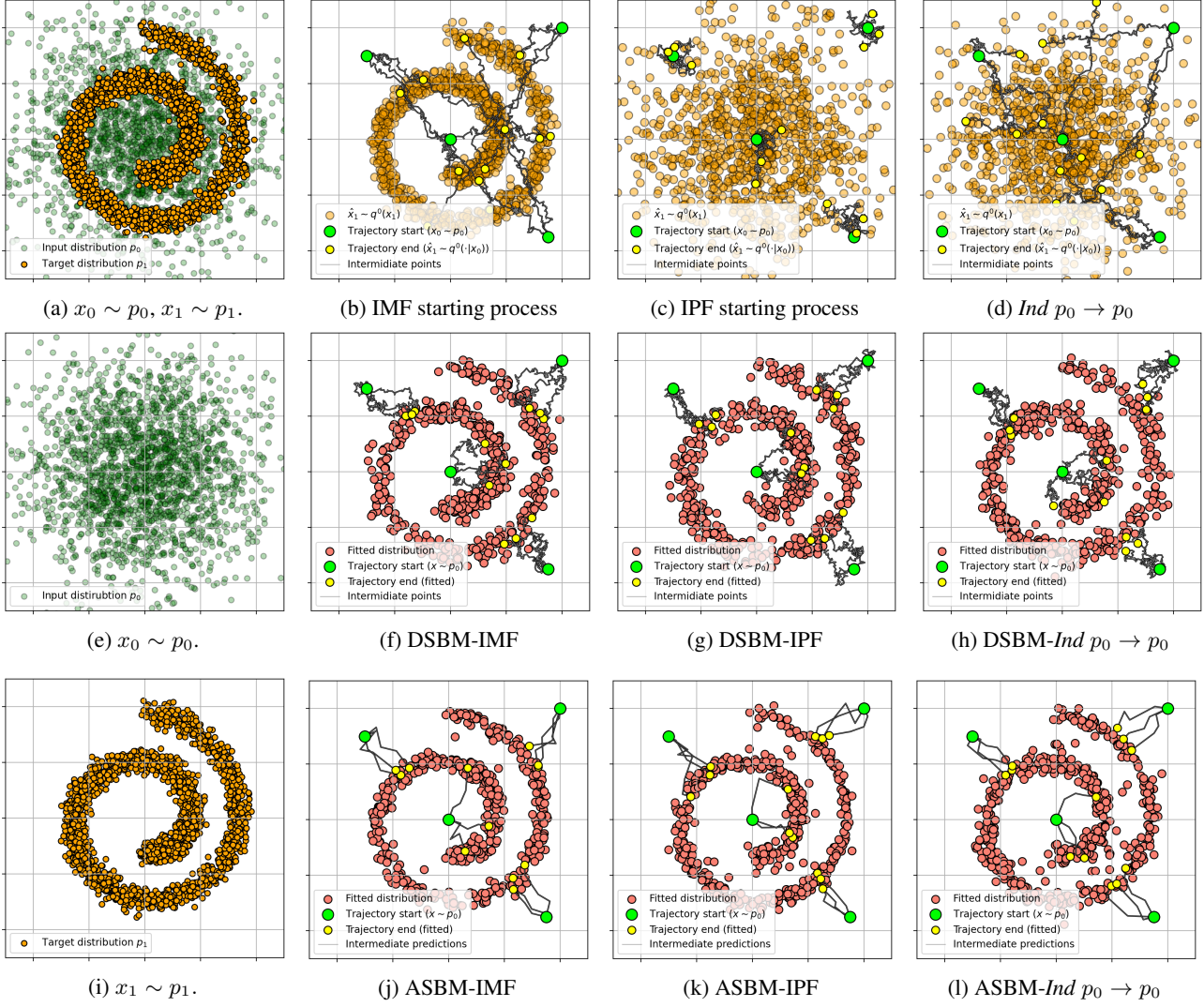


Figure 7: Visualization of learned processes with DSBM and ASBM solvers for *Gaussian* \rightarrow *Swiss roll* translation using IMF, IPF, *Ind* $p_0 \rightarrow p_0$ starting processes for $\epsilon = 0.1$.

C.5. General experimental details

Authors of ASBM (Gushchin et al., 2024) kindly provided us the code for all the experiments. All the hyperparameters including neural networks architectures were chosen as close as possible to the ones used by the authors of ASBM in their experimental section. Particularly, as it is described in (Gushchin et al., 2024, Appendix D), authors used DD-GAN (Xiao et al.) with Brownian Bridge posterior sampling instead of DDPM’s one and implementation from:

<https://github.com/NVlabs/denoising-diffusion-gan>

DSBM (Shi et al., 2023) implementation is taken from the official code repository:

<https://github.com/yuyang-shi/dsbm-pytorch>

Sampling on the inference stage is done by Euler Maryama SDE numerical solver (Kloeden, 1992) with indicated in Table 3 NFE.

Ind $p_0 \rightarrow p_0$ starting process in all the experiments was implemented in mini batch manner, i.e., $\{x_{0,n}\}_{n=1}^N \sim p_0$ and x_1 batch $\{x_{1,n}\}_{n=1}^N \sim q^0(\cdot|\{x_{0,n}\}_{n=1}^N)$ is generated by permutation of $\{x_{0,n}\}_{n=1}^N$ mini batch indices.

The Exponential Moving Average (EMA) has been used to enhance generator’s training stability of both ASBM and

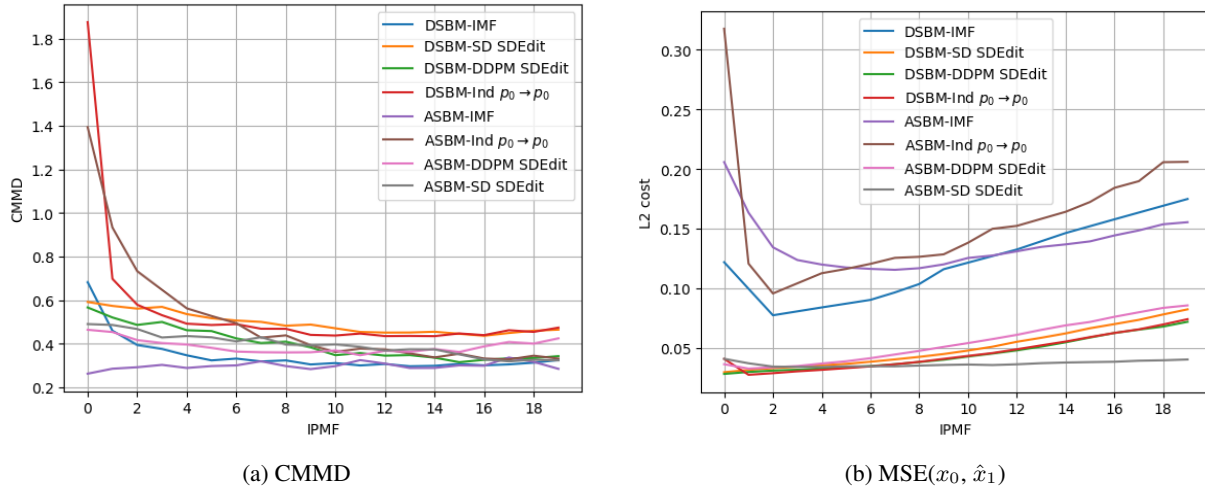


Figure 8: Test metrics in Celeba $male \rightarrow female$ (64×64) as a function of IPMF iteration for various starting couplings.

Model	Dataset	Start process	IPMF iters	IPMF-0 Grad Updates	IPMF-k Grad Updates
ASBM	Celeba	All	20	200000	20000
DSBM	Celeba	All	20	100000	20000
ASBM	Swiss Roll	All	20	400000	40000
DSBM	Swiss Roll	All	20	20000	20000
ASBM	cMNIST	All	20	75000	38000
DSBM	cMNIST	All	20	100000	20000
ASBM	SB Bench	All	20	133000	67000
DSBM	SB Bench	All	20	20000	20000

Model	Dataset	Start process	NFE	EMA decay	Batch size	D/G opt ratio	Lr G	Lr D
ASBM	Celeba	All	4	0.999	32	1:1	1.6e-4	1.25e-4
DSBM	Celeba	All	100	0.999	64	N/A	1e-4	N/A
ASBM	Swiss Roll	All	4	0.999	512	1:1	1e-4	1e-4
DSBM	Swiss Roll	All	100	N/A	128	N/A	1e-4	N/A
ASBM	cMNIST	All	4	0.999	64	2:1	1.6e-4	1.25e-4
DSBM	cMNIST	All	30	0.999	128	N/A	1e-4	N/A
ASBM	SB Bench	All	32	0.999	128	3:1	1e-4	1e-4
DSBM	SB Bench	All	100	N/A	128	N/A	1e-4	N/A

Table 3: Hyperparameters of models from Celeba 4.4, SwissRoll 4.2, cMNIST 4.4 and Benchmark 4.3 experiments. In "Start process" the column "All" states for all the used options. "N/A" corresponds to either not used or not applicable corresponding option.

DSBM. The parameters of the EMA are provided in Table 3, in case the EMA decay is set to "N/A" no averaging has been applied.

C.6. Illustrative 2D examples details

ASBM. For toy experiments the MLP with hidden layers [256, 256, 256] has been chosen for both discriminator and generator. The generator takes vector of $(dim + 1 + 2)$ length with data, latent variable and embedding (a simple lookup table `torch.nn.Embedding`) dimensions, respectively. The networks have `torch.nn.LeakyReLU` as activation layer with 0.2 angle of negative slope. The optimization has been conducted using `torch.optim.Adam` with running averages coefficients 0.5 and 0.9. Additionally, the `CosineAnnealingLR` scheduler has been used only at pretraining iteration with minimal learning rate set to $1e-5$ and no restarting. To stabilize GAN training R1 regularizer with coefficient 0.01 (Mescheder et al., 2018) has been used.

DSBM. MLP with $[dim + 12, 128, 128, 128, 128, 128, dim]$ number of hidden neurons, `torch.nn.SiLU` activation functions, residual connections between 2nd/4th and 4th/6th layers and Sinusoidal Positional Embedding has been used.

C.7. SB benchmark details

Scrödinger Bridges/Entropic Optimal Transport Benchmark (Gushchin et al., 2023b) and cBW_2^2 -UVP, BW_2^2 -UVP metric implementation was taken from the official code repository:

<https://github.com/ngushchin/EntropicOTBenchmark>

Conditional plan metric cBW_2^2 -UVP, see Table 1, was calculated over predefined test set and conditional expectation per each test set sample estimated via Monte Carlo integration with 1000 samples. Target distribution fitting metric, BW_2^2 -UVP, see Table 2, was estimated using Monte Carlo method and 10000 samples.

ASBM. The same architecture and optimizer have been used as in toy experiments C.6, but without the scheduler.

DSBM. MLP with $[\text{dim} + 12, 128, 128, 128, 128, 128, \text{dim}]$ number of hidden neurons, `torch.nn.SiLU` activation functions, residual connections between 2nd/4th and 4th/6th layers and Sinusoidal Positional Embedding has been used.

C.8. CMNIST details

Working with MNIST dataset, we use regular train/test split with 60000 images and 10000 images correspondingly. We RGB color train and test digits of classes "2" and "3". Each sample is resized to 32×32 and normalized by 0.5 mean and 0.5 std.

ASBM. The cMNIST setup mainly differs by the architecture used. The generator model is built upon the NCSN++ architecture (Song et al.), following the approach in (Xiao et al.) and (Gushchin et al., 2024). We use 2 residual and attention blocks, 128 base channels, and $(1, 2, 2, 2)$ feature multiplications per corresponding resolution level. The dimension of the latent vector has been set to 100. Following the best practices of time-dependent neural networks sinusoidal embeddings are employed to condition on the integer time steps, with a dimensionality equal to $2 \times$ the number of initial channel, resulting in a 256-dimensional embedding. The discriminator adopts ResNet-like architecture with 4 resolution levels. The same optimizer with the same parameters as in toy C.6 and SB benchmark C.7 experiments have been used except ones that are presented in Table 3. No scheduler has been applied. Additionally, R1 regularization is applied to the discriminator with a coefficient of 0.02, in line with (Xiao et al.) and (Gushchin et al., 2024).

DSBM. The model is based on the U-Net architecture (Ronneberger et al., 2015) with attention blocks, 2 residual blocks per level, 4 attention heads, 128 base channels, $(1, 2, 2, 2)$ feature multiplications per resolution level. Training was held by Adam (Kingma & Ba, 2014) optimizer.

C.9. Celeba details

Test FID, see Figure 6 is calculated using `pytorch-fid` package, test CMMD is calculated using unofficial implementation in PyTorch. Working with CelebA dataset (Liu et al., 2015), we use all 84434 male and 118165 female samples (90% train, 10% test of each class). Each sample is resized to 64×64 and normalized by 0.5 mean and 0.5 std.

ASBM. As in cMNIST experiments C.8 the generator model is built upon the NCSN++ architecture (Song et al.) but with small parameter changes. The number of initial channels has been lowered to 64, but the number of resolution levels has been increased with the following changes in feature multiplication, which were set to $(1, 1, 2, 2, 4)$. The discriminator also has been upgraded by growing the number of resolution levels up to 6. No other changes were proposed.

DSBM. Following Colored MNIST translation experiment exactly the same neural network and optimizer was used.

SDEdit coupling. DDPM (Ho et al., 2020) was trained on Celeba female train part processed in the same way as for other Celeba experiments. Number of diffusion steps is equal to 1000 with linear β_t noise schedule, number of training steps is equal to 1M, UNet (Ronneberger et al., 2015) was used as neural network with 78M parameters, EMA was used during training with rate 0.9999. The DDPM code was taken from the official DDIM (Song et al., 2020) github repository:

<https://github.com/ermongroup/ddim>

The SDEdit method (Meng et al., 2021) for DDPM model was used with 400 steps of noising and 400 steps of denoising. The code for SDEdit method was taken from the official github repository:

<https://github.com/ermongroup/SDEdit>

The Stable Diffusion V1.5 (Rombach et al., 2022) model was taken from the Huggingface (Wolf et al., 2020) model hub with the tag *"runwayml/stable-diffusion-v1-5"*. The text prompt used is *"A female celebrity from CelebA"*. The SDEdit method implementation for the SDv1.5 model was taken from the Huggingface library (Wolf et al., 2020), i.e. *"StableDiffusionImg2ImgPipeline"*, with hyperparameters: *strength 0.75, guidance scale 7.5, number of inference steps 50*. The output of SDEdit pipeline has been downscaled from 512×512 size to 64×64 size using bicubic interpolation.